

# Probing Reheating Phase via Non-Helical Magnetogenesis and Secondary Gravitational Waves

Subhasis Maiti<sup>\*</sup> and Debaprasad Maity<sup>†</sup>

*Department of Physics, Indian Institute of Technology, Guwahati, Assam, India*

Rohan Srikanth<sup>‡</sup>

*Institut für Physik und Astronomie, Universität Potsdam,  
Haus 28, Karl-Liebknecht-Str. 24/25, 14476, Potsdam, Germany*

(Dated: June 10, 2025)

In the past two decades, significant advancements have been made in observational techniques to enhance our understanding of the universe and its evolutionary processes. However, our knowledge of the post-inflation reheating phase remains limited due to its small-scale dynamics. Traditional observations, such as those of the Cosmic Microwave Background (CMB), primarily provide insights into large-scale dynamics, making it challenging to glean information about the reheating era. In this paper, our primary aim is to explore how the generation of Gravitational Waves (GWs) spectra, resulting from electromagnetic fields in the early universe, can offer valuable insights into the Reheating dynamics. We investigate how the spectral shape of GWs varies across different frequency ranges, depending on the initial magnetic profile and reheating dynamics. For this, we consider a well-known non-helical magnetogenesis model, where the usual electromagnetic kinetic term is coupled with a background scalar. Notably, for such a scenario, we observe distinct spectral shapes with sufficiently high amplitudes for different reheating histories with the equation of state parametrized by  $(w_{\text{re}})$ . We identify spectral breaks in the GW spectra for both  $w_{\text{re}} < 1/3$  and  $w_{\text{re}} > 1/3$  scenarios. We find that future GW experiments such as BBO, LISA, SKA, and DECIGO are well within the reach of observing those distinct spectral shapes and can potentially shed light on the underlying mechanism of the reheating phase. Finally, we attempt to constrain the non-helical models under consideration utilizing the latest NANOGrav 15-year observation campaign. We find that in order to explain the observed GW spectrum in the nano-Hz range, the required magnetic field spectrum needs to be very stiff. However, such a stiff magnetic field spectrum in turn yields a strongly blue-tilted GW spectrum, which is in conflict with other cosmological observations.

PACS numbers:

## I. INTRODUCTION:

The last decade can be called *the* era of Gravitational waves (GW) in the field of observational cosmology. Despite its long-standing prediction undergoing painstaking conceptual checks in Einstein's General Relativity framework, detection of GW was close to impossible till the LIGO-Virgo collaboration detected the GW signal from a distant source of merging black hole binary in 2015 [1–5]. Subsequently, within ten years, a large number of GW sources have been detected along with the latest revelation of stochastic GW background in the Nano-Hertz frequency range decoded from the measured tiny variation of the periods of Pulsar Timing Arrays (PTA) scattered in the sky [6–10]. Except for different classes of precisely known astrophysical binary sources, stochastic Nano-Hz GW sources are not easy to identify. And this certainly signals the beginning of an era of GWs starting to play their long-expected role in revealing the mystery of the early universe.

The mechanism of producing stochastic GW has been the subject of intensive theoretical investigation over several decades in theoretical cosmology. Primordial stochastic gravitational waves (PSGWs) are an ideal probe for studying the early universe's dynamics and microscopic physics due to their pristine nature. These waves are hypothesized to have originated from the quantum vacuum and amplified by the inflationary mechanism. The detection of PSGWs would not only validate the inflationary mechanism but also provide crucial insights

---

<sup>\*</sup>Electronic address: E-mail: [subhashish@iitg.ac.in](mailto:subhashish@iitg.ac.in)

<sup>†</sup>Electronic address: E-mail: [debu@iitg.ac.in](mailto:debu@iitg.ac.in)

<sup>‡</sup>Electronic address: E-mail: [rohan.srikanth@uni-potsdam.de](mailto:rohan.srikanth@uni-potsdam.de)

into physics at extremely high energy scales. PSGWs are generated from the inflationary quantum vacuum, and their production and evolution have been extensively studied in the literature [11–14].

Inflation is a well-established mechanism in which spacetime vacuum fluctuations are amplified, leading to the generation of tensor perturbations without the need for external sources. The gravitational waves (GWs) produced from these vacuum fluctuations are referred to as primary gravitational waves (PGWs) [11–14]. In our model, electromagnetic (EM) fields are also generated during inflation. It is well known that such EM fields can act as efficient sources of secondary gravitational waves (SGWs) [15–28]. Unlike PGWs, SGWs carry imprints not only of the background dynamics but also of the intrinsic properties of their sources. In this work, we focus on the production and evolution of SGWs sourced by inflationary electromagnetic fields, with particular emphasis on the effects of the reheating phase. Our analysis considers a specific class of electromagnetic sources assumed to originate from inflationary magnetogenesis.

Studies on inflationary magnetogenesis [17, 29–42] has mostly focused on producing large-scale magnetic field (LSMF) in the intergalactic medium in voids ( $\sim 10^{-16}$  Gauss of coherence length as large as Mpc scales) as hinted by different observations [43–45]. Furthermore, such large-scale magnetic fields are also argued to act as a tiny seed initial magnetic field which may be amplified by the well-known galactic dynamo mechanism [46–49] to produce magnetic fields at various astrophysical and galactic scales of order a few micro Gauss [30, 49, 50]. Non-linear magneto-hydrodynamic effects at astrophysical and galactic scales generically erase the detailed properties of the initial seed field, which makes it difficult to verify such inflationary mechanisms of magnetogenesis models. Moreover, magnetic fields in the voids of the Mpc scale are extremely challenging to detect. Apart from the indirect  $\gamma$ -ray observational lower limit of LSMF setting some constraints [51–53], all the magnetogenesis models are largely unconstrained and poorly understood from the observational point of view. Therefore, it is essential to look for some indirect observables that can help understand such mechanisms better. In this realm, studies have been performed on the physical effect of LSMF on various important cosmological observables such as inflationary power spectrum [54], CMB [55, 56], gravitational waves [15, 16, 18–20]. In this paper, we shall study in detail the production of SGW due to the electromagnetic field produced during inflation. As we shall observe, the SGW dynamics and its spectrum crucially depend on the magnetogenesis model and the background evolution. Therefore, SGW naturally encodes the physics of inflation and the magnetogenesis models together.

After the end of inflation [57–61], both GWs and the produced electromagnetic field will evolve through a reheating phase which depends on the very nature of the inflaton field near its minimum and how it is coupled to the standard model fields. In the simplest perturbative framework, this phase is parametrized by the reheating temperature ( $T_{\text{re}}$ ) which encodes inflaton decay width,  $\Gamma$  into standard model fields through the relation  $T_{\text{re}} \propto \sqrt{\Gamma}$ , and the inflation equation of state ( $w_{\text{re}}$ ) which encodes the nature of the inflaton potential [62–68]. Even though the reheating temperature is broadly bounded within  $10^{15}\text{GeV} > T_{\text{re}} > T_{\text{BBN}} \sim 10\text{ MeV}$  [69, 70], the inflaton/reheating equation of state is mostly unconstrained (see recent works on this [70]). A recent surge of activity on understanding this phase has been to realize the underlying connection among inflationary parameters such as scalar spectral index ( $n_s$ ) and the reheating parameters ( $T_{\text{re}}, w_{\text{re}}$ ) [70–73]. Furthermore, the evolution of PGW has also been shown to encode valuable information when passing through this phase, see [14] and references therein. In this paper, we will analyze in detail the production of SGW, a specific class of non-helical magnetogenesis scenario accounting for the observable constraints on the present-day LSMF combined with the CMB anisotropies, BBN, and other sensitivity curves of the future observatories. Our SGW analysis is observed to put interesting constraints on the nature of inflation through its equation of state  $w_{\text{re}}$ , reheating temperature  $T_{\text{re}}$ , and the inflationary magnetogenesis model itself. To generate the LSMF, we consider a simple model of primordial magnetogenesis with the coupling  $f^2(\phi)FF$  [33–36].

The structure of the paper is organized as follows. In Section II, we present a detailed analysis of the primordial magnetic fields generated during inflation, emphasizing the impact of non-trivial reheating dynamics. In particular, we investigate how the presence of conductivity during reheating can significantly influence the present-day strength of magnetic fields on large scales. In Section III, we explore how the presence of electromagnetic fields modifies the gravitational wave (GW) spectrum under generalized reheating dynamics, and discuss the prospects for detecting these signals with future GW observatories. Section IV is devoted to presenting key results from our analysis of the GW spectral features, along with constraints on the reheating dynamics derived from both the tensor-to-scalar ratio bounds and the limits on  $\Delta N_{\text{eff}}$  bound. Finally, in Section V, we summarize our main findings and conclude.

## II. MAGNETOGENESIS: QUANTIZING THE GAUGE FIELD AND EVOLUTION OF ITS POWER SPECTRUM

To make our paper self-contained, we briefly describe the quantization of gauge fields and define the associated spectrum in the FLRW background. Maxwell's theory in four dimensions is conformally invariant, which means that to generate magnetic fields in a spatially flat universe as discussed in [17, 32–36, 39–41], one must break conformal invariance. To achieve this, a time-dependent effective gauge coupling  $f(\eta)$  is typically introduced [32–36].

$$\mathcal{S}_{\text{EM}} = -\frac{1}{4} \int d^4x \sqrt{-g} g^{\alpha\beta} g^{\mu\nu} f^2(\eta) F_{\mu\alpha} F_{\nu\beta}. \quad (1)$$

Where  $F_{\mu\nu} = \partial_\mu A_\nu - \partial_\nu A_\mu$ , is the electromagnetic field tensor and  $A_\mu$  is four-vector potential. The possible source of the gauge coupling  $f(\eta)$  will not be discussed here and will be taken up in our future publication. Here, we will follow the quantization procedure discussed in the paper [74]. Throughout this analysis, we will treat electromagnetic field perturbatively compared to inflation and radiation energy density, i.e.,  $\rho_{em}/\rho_{inf}, \rho_{em}/\rho_{rad} < 1$ , and spatially Flat FLRW metric background in conformal coordinates is

$$ds^2 = g_{\mu\nu} dx^\mu dx^\nu = a^2(\eta)(-d\eta^2 + dx^2), \quad (2)$$

where ‘ $\eta$ ’ is the conformal time. Spatial flatness helps us to denote the vector potential in terms of irreducible components as  $A_\mu = (A_0, \partial_i S + A_i)$  with the traceless condition  $\delta^{ij} \partial_i A_j = 0$ . In terms of these components the action Eq.(1) becomes,

$$\mathcal{S}_{\text{EM}} = \frac{1}{2} \int d\eta d^3x f(\eta)^2 (A'_i A^{i'} - \partial_i A_j \partial^i A^j). \quad (3)$$

Because of the inherent conformal invariance, the action becomes independent of the scale factor. The spatial index will be raised or lowered by the usual Kronecker delta function. Assuming the Fourier expansion of  $A_i$  as

$$A_i(\eta, \mathbf{x}) = \sum_{\lambda=1,2} \int \frac{d^3k}{(2\pi)^3} \epsilon_i^\lambda(\mathbf{k}) e^{i\mathbf{k}\cdot\mathbf{x}} u_k^\lambda(\tau), \quad (4)$$

with the reality condition  $u_{-\mathbf{k}}^\lambda = u_{\mathbf{k}}^{\lambda*}$ , the polarization vector  $\epsilon_i^\lambda(\mathbf{k})$  corresponding to two modes  $\lambda = 1, 2$ , and satisfies  $\epsilon_i^\lambda(\mathbf{k}) k_i = 0$  and  $\epsilon_i^\lambda(\mathbf{k}) \epsilon_i^{\lambda'}(\mathbf{k}) = \delta_{\lambda\lambda'}$ . The associated mode function satisfies [35, 36],

$$u_{\mathbf{k}}^{\lambda''} + 2 \frac{f'}{f} u_{\mathbf{k}}^{\lambda'} + k^2 u_{\mathbf{k}}^\lambda = 0, \quad (5)$$

where the prime denotes the derivative with respect to the conformal time  $\eta$ . The electric and magnetic power spectrum in terms of the mode function is written as,

$$\mathcal{P}_E = \frac{f^2 k^3}{4\pi^2 a^4} \sum_{\lambda=\pm} |u_{\mathbf{k}}^{\lambda'}|^2 \quad ; \quad \mathcal{P}_B = \frac{f^2 k^5}{4\pi^2 a^4} \sum_{\lambda=\pm} |u_{\mathbf{k}}^\lambda|^2. \quad (6)$$

Power spectrum can now be computed once we know the mode function  $u_{\mathbf{k}}^\lambda$  for a given inflationary and magnetogenesis model. Since,  $(\mathcal{P}_E, \mathcal{P}_B)$  are connected to the direct physically measurable quantities, we chose to take a slightly different but transparent approach by directly solving the equations for comoving power spectrum  $(\mathcal{P}_E^c = (a^4/f^2)\mathcal{P}_E, \mathcal{P}_B^c = (a^4/f^2)\mathcal{P}_B)$  as

$$\begin{aligned} \mathcal{P}_E^{c'} + 4 \frac{f'}{f} \mathcal{P}_E^c &= -\mathcal{P}_B^{c'} \\ \mathcal{P}_B^{c''} + 2 \frac{f'}{f} \mathcal{P}_B^{c'} + 2k^2 \mathcal{P}_B^c &= 2k^2 \mathcal{P}_E^c. \end{aligned} \quad (7)$$

The above equations clearly state that once the comoving magnetic power spectrum  $\mathcal{P}_B^c$  is known,  $\mathcal{P}_E^c$  can be automatically obtained from the second equation, and vice versa. Hence, it is sufficient to set the initial condition for the comoving magnetic spectrum,  $\mathcal{P}_B^c|_{-k\tau \rightarrow \infty} = k^4/4\pi^2 f^2$ , which can be obtained by explicitly solving for the electromagnetic mode function, (Eq.5) for  $u_{\mathbf{k}}^\lambda$ , and applying both the Bunch-Davis (BD) vacuum and normalization conditions, namely  $u_{\mathbf{k}}^\lambda|_{\text{BD}} = 1/(\sqrt{2k f^2}) e^{-ik\eta}$ .

### A. Defining Reheating Temperature and Inflationary Parameters

In the standard cosmological model, inflation is followed by a phase of reheating, during which energy is transferred from the inflaton field to radiation. This phase is characterized by the mass of the inflaton, its self-coupling, and its coupling to radiation. In the perturbative regime, these parameters can be related to the equation-of-state (EoS) parameter  $w_{re}$  and the reheating temperature  $T_{re}$ .

During reheating, the energy density of the inflaton evolves as  $a^{-3(1+w_{re})}$  since the inflaton field dominates this phase. The reheating temperature,  $T_{re}$ , is defined as the point at which the energy densities of the inflaton ( $\rho_\phi$ ) and radiation ( $\rho_r$ ) become equal. To maintain a model-independent approach, we consider the EoS ( $w_{re}$ ) and the reheating temperature ( $T_{re}$ ) as free parameters.

The duration of the reheating period can be quantified by the total number of e-folds during reheating, denoted as  $N_{re}$ , and is given by [71, 75]

$$N_{re} = \frac{1}{3(1+w_{re})} \ln \left( \frac{90H_1^2 M_P^2}{\pi^2 g_{re} T_{re}^4} \right). \quad (8)$$

Here,  $H_1$  is the Hubble parameter during inflation, assumed to remain constant throughout the inflationary era. The reduced Planck mass is  $M_P = 1/\sqrt{8\pi G} \simeq 2.14 \times 10^{18}$  GeV, and  $g_{re} \simeq 106.7$  represents the number of relativistic degrees of freedom at the beginning of the radiation-dominated era.

We can also define other relevant parameters as follows [75]:

$$k_{re} \simeq 3.9 \times 10^6 \left( \frac{T_{re}}{10^{-2} \text{ GeV}} \right) \text{ Mpc}^{-1}, \quad (9)$$

where  $k_{re}$  represents the lowest mode that can re-enter the horizon before the end of reheating.

Additionally, we define  $k_e$  as [75]

$$k_e = \left( \frac{43g_{re}}{11} \right)^{1/3} \left( \frac{\pi^2 g_{re}}{90} \right)^\alpha \frac{H_1^{1-2\alpha} T_{re}^{4\alpha-1} T_0}{M_P^{2\alpha}}, \quad (10)$$

where  $\alpha = 1/3(1+w_{re})$  and  $T_0 = 2.725$  K is the present-day CMB temperature. Here, we consider  $a_0 = 1$  as the present-day value of the scale factor.

### B. Evolution of electromagnetic power spectrum through different phases

Our main objective is to trace the evolution of the electromagnetic power spectrum from the inflationary period to the current era and then compare it with the observed limit on the magnetic power spectrum. To this end, we will examine the gravitational wave power spectrum's development in the presence of this electromagnetic source.

#### 1. Evolution During inflation:

During Inflation, we assume the ansatz for the gauge coupling function as [34–36]

$$f(\eta) = \begin{cases} \left( \frac{a}{a_{end}} \right)^n & \text{for } a \leq a_{end} \\ 1 & \text{for } a > a_{end} \end{cases}. \quad (11)$$

Note that after the end of inflation set at  $a_{end}$ , the coupling function becomes unity, which restores the usual conformal symmetry of the electromagnetic field.

To solve for the spectrum analytically, we further assumed inflation to be approximately de Sitter type, and with this assumption, the scale factor behaves as  $a = -1/H_1 \eta$ , where  $H_1$  is the Hubble constant. With the above choice of gauge coupling function, one can easily obtain the analytic solution for the magnetic power spectrum as

$$\mathcal{P}_B^c = (a^4/f^2) \mathcal{P}_B = (-k\eta)^{1+2n} (c_1 H_{n+\frac{1}{2}}(k\eta)^2 + c_2 |H_{n+\frac{1}{2}}(k\eta)|^2 + c_3 H_{n+\frac{1}{2}}^*(k\eta)^2). \quad (12)$$

Where  $c_1, c_2, c_3$  are the integration constants, and  $(H_{n+1/2}, H_{n+1/2}^*)$  are the Hankel functions of the first kind and their complex conjugate. The electric power spectrum can be easily computed from Eq.(7). Since, in the asymptotic past limit,  $a^4 \mathcal{P}_B^c|_{-k\eta \rightarrow \infty} = k^4/4\pi^2 f^2$ , one obtains the integration constants to be

$$c_1 = c_3 = 0 ; \quad c_2 = \frac{k^4}{8\pi} \left( \frac{1}{-k\eta_{end}} \right)^{2n}. \quad (13)$$

Once we obtain the expression for  $\mathcal{P}_B^c$ , the corresponding electric counterpart can be obtained from Eq.(7), and using Eq. (13), we get the final expressions for the electromagnetic power spectrum [35] as,

$$\mathcal{P}_B^{\text{inf}}(k, \eta) = \frac{d\rho_B}{d\ln(k)} = \frac{k^4}{8\pi a^4(\eta)} (-k\eta) \left| H_{n+\frac{1}{2}}^{(1)}(-k\eta) \right|^2, \quad (14)$$

$$\mathcal{P}_E^{\text{inf}}(k, \eta) = \frac{d\rho_E}{d\ln(k)} = \frac{k^4}{8\pi a^4(\eta)} (-k\eta) \left| H_{n-\frac{1}{2}}^{(1)}(-k\eta) \right|^2. \quad (15)$$

To analyse the power spectrum's characteristics at the super-horizon scale, where all the relevant modes are well outside the Hubble radius at the end of inflation, we consider the limit where  $k/aH_1 \ll 1$ . Depending on the sign of  $n$ , we can express the electric and magnetic power spectrum in a simpler form, as explained in [33, 35, 36]

$$\left. \begin{aligned} \mathcal{P}_B^{\text{inf}}(k, \eta) &= \frac{H_1^4}{8\pi} \frac{2^{2|n|+1} \Gamma^2(|n|+\frac{1}{2})}{\pi^2} (-k\eta)^{-2|n|+4} \\ \mathcal{P}_E^{\text{inf}}(k, \eta) &= \frac{H_1^4}{8\pi} \frac{\Gamma^2(|n|-\frac{1}{2}) 2^{2|n|-1}}{\pi^2} (-k\eta)^{-2|n|+6} \end{aligned} \right\} \text{ for } n > \frac{1}{2}, \quad (16)$$

$$\left. \begin{aligned} \mathcal{P}_B^{\text{inf}}(k, \eta) &= \frac{H_1^4}{8\pi} \frac{\Gamma^2(|n|-\frac{1}{2}) 2^{2|n|-1}}{\pi^2} (-k\eta)^{-2|n|+6} \\ \mathcal{P}_E^{\text{inf}}(k, \eta) &= \frac{H_1^4}{8\pi} \frac{2^{2|n|+1} \Gamma^2(|n|+\frac{1}{2})}{\pi^2} (-k\eta)^{-2|n|+4} \end{aligned} \right\} \text{ for } n < -\frac{1}{2}. \quad (17)$$

After obtaining the power spectrum during inflation, we can use it as a boundary condition to solve for the power spectrum during reheating. It is important to note that for  $n > 1/2$ , the ratio of two strength turned out to be  $\mathcal{P}_B^{\text{inf}}(k)/\mathcal{P}_E^{\text{inf}}(k) \propto (k\eta)^{-2} \gg 0$ . This immediately suggests that at the end of inflation, the magnetic (electric) field strength dominates over the electric (magnetic) field strength for  $n > 1/2 (< -1/2)$ . To estimate the magnetic field strength at the end of inflation for a specific set of parameters, we consider an inflationary energy scale of  $H_1 \simeq 10^{-5} M_{\text{P}}$  and an inflationary duration corresponding to  $N_1 = 55$  e-folds. For  $n = 2$ , which corresponds to a scale-invariant magnetic spectrum, the field strength at a comoving scale of  $k = 1 \text{ Mpc}^{-1}$  is found to be  $B_{n=2}(1 \text{ Mpc}^{-1}) \simeq 10^{46} \text{ G}$ . In contrast, for  $n = -2$ , where the magnetic spectrum exhibits a scale-dependent behavior with  $B_{n=-2} \propto k$ , the field strength at the same scale is estimated as  $B_{n=-2}(1 \text{ Mpc}^{-1}) \simeq 10^{23} \text{ G}$ . Notably, for scale-dependent spectra, the field strength is influenced by the duration of inflation due to the factor  $(k/k_e)^{n_B}$ , whereas for scale-invariant spectra, it remains independent of the inflationary duration.

*a. Results for Inflationary Magnetogenesis:* The strength of the electromagnetic power spectrum at the end of inflation is governed by equations (16),(17). Assuming an instantaneous reheating scenario, and the inflationary Hubble parameter  $H_1 \simeq 10^{-5} M_{\text{P}}$ , we can determine the present-day magnetic field strength as follows:

$$B_0(k) \simeq 1.84 \times 10^{-12} \text{ G} \left( \frac{k}{k_e} \right)^{2-|n|} \times \begin{cases} 2^{n+\frac{1}{2}} \Gamma(n+\frac{1}{2}) & \text{for } n > 1/2 \\ 2^{n-\frac{1}{2}} \Gamma(n-\frac{1}{2}) \frac{k}{k_e} & \text{for } n < -1/2 \end{cases}. \quad (18)$$

Notably, the case of  $n = 2$  yields a scale-invariant magnetic field. Despite the scale-invariance, it faces the challenge of the strong coupling problem due to the large effective electromagnetic gauge coupling  $\propto 1/f^2$ , at the onset of inflation. However, it can generate a magnetic field strength of around  $\sim 10^{-11} \text{ G}$ . Note that such a strong magnetic field can have a sizable impact on the tensor-to-scalar ratio, which we will discuss in the GW section. On the other hand, the  $n = -2$  coupling leads to a scale-dependent magnetic field strength is  $B_0(1 \text{ Mpc}^{-1}) \simeq 1.45 \times 10^{-36} \text{ G}$ , which is very small compared with the current observational bound on the 1 Mpc scale [43–45].

*b. Backreaction of Electromagnetic Fields:* Including the coupling function  $f(\eta)$  in Eq. (1) facilitates electromagnetic (EM) field generation during inflation, resulting in a total post-inflation energy density  $\rho_{\text{total}} = \rho_c^I + \rho_{\text{em}}^I$ , where  $\rho_c^I = 3H_I^2 M_P^2$  is the inflaton energy density and electromagnetic energy density

$$\rho_{\text{em}}^I = \int_{k_*}^{k_e} d\ln(k) \times \mathcal{P}_{\text{B/E}}(k, \eta_e) \simeq \frac{H_I^4}{8\pi} \frac{2^{2|n|+1} \Gamma^2(|n| + \frac{1}{2})}{\pi^2} \frac{(1 - (k_*/k_e)^{n_{\text{B/E}}})}{n_{\text{B/E}}}. \quad (19)$$

Where  $n_{\text{B/E}} = 4 - 2|n|$ , represent the spectral indices of the electromagnetic (EM) fields, and  $k_*$  is the CMB pivot scale. From Eqs. (14), the spectrum is blue-tilted for  $|n| < 2$  and red-tilted for  $|n| > 2$ . For scenarios with  $|n| \leq 2$ , therefore,  $\rho_{\text{em}} \propto H_I^4$ . In contrast, for  $|n| > 2$ ,  $\rho_{\text{em}} \propto H_I^4 (k_e/k_*)^{|n_{\text{B/E}}|}$ , which depends not only on the inflationary energy scale but also on the duration of the inflationary era.

When the energy density of the EM field approaches that of the inflaton, backreaction effects on the background evolution can become significant, affecting expansion dynamics and the power spectrum of primordial perturbations. To quantify this, we define the parameter  $\zeta^I = \rho_{\text{em}}^I / \rho_c^I$ , providing a measure of the EM field's influence relative to the background energy. At the end of inflation, the fractional energy density  $\zeta^I$  is defined as

$$\zeta^I \simeq 3.98 \times 10^{-12} \left( \frac{H_I}{10^{-5} M_P} \right)^2 2^{n+\frac{1}{2}} \Gamma(n + \frac{1}{2}) \frac{1 - e^{-n_{\text{B/E}} N_I}}{n_{\text{B/E}}}, \quad (20)$$

When  $\zeta^I = 1$ , the EM energy density becomes comparable to that of the inflationary background, signaling the onset of significant backreaction. For an instantaneous reheating scenario with  $N_I = 55$ , with  $H_I \simeq 10^{-5} M_P$ , we find that to avoid backreaction, the index parameter must satisfy  $|n| \leq 2.18$ . This value depends on the inflationary model, as the duration of inflation affects  $k_e$ , which is given by  $k_e = k_* \exp[N_I]$ .

In the subsequent subsection, we discuss how post-inflationary dynamics, particularly reheating, affect the evolution of primordial magnetic fields. We focus on the role of electrical conductivity during reheating, which plays a crucial role in determining the fate of the generated fields. For simplicity, we consider two extreme scenarios, one with vanishing electrical conductivity and another with very large electrical conductivity. Here we are going to discuss how the zero electrical conductivity limit, the conversion of the electric energy to magnetic energy, can help us to explain the current day observed magnetic field strength at large scale for  $n < -1/2$ , where the model does not have any kind of backreaction and strong coupling issue.

## 2. Evolution During reheating:

Given the assumption of the gauge coupling function  $f(\eta) = 1$  (see Eq.(11)) after the end of inflation  $a > a_{\text{end}}$ , the evolution equation for the comoving electromagnetic power spectrum during reheating will become

$$\mathcal{P}_E^{c'} = -\mathcal{P}_B^{c'} \quad (21a)$$

$$\mathcal{P}_B^{c''} + 2k^2 \mathcal{P}_B^c = 2k^2 \mathcal{P}_E^c. \quad (21b)$$

Note that the above equations do not explicitly depend on the scale factor, and that is due to the underlying conformal invariance of the gauge fields. During reheating, there is no coupling term to break the invariance like the one in Eq.(1). So, we can identify the solutions of Eqs(21) as comoving electric and magnetic power spectrum defined as  $\mathcal{P}_B^c = a^4 \mathcal{P}_B$  and  $\mathcal{P}_E^c = a^4 \mathcal{P}_E$ . And the solution of the Eqs(21) is governed by

$$a^4 \mathcal{P}_B = \frac{d_2}{2} + d_1 \cos(2k(\eta - \eta_{\text{end}})), \quad (22a)$$

$$a^4 \mathcal{P}_E = \frac{d_2}{2} - d_1 \cos(2k(\eta - \eta_{\text{end}})) \quad (22b)$$

where  $d_1, d_2$  are the constants, which can be fixed by providing proper initial conditions at the end of inflation, and we get the following expressions,

$$d_1 = \frac{\mathcal{B} - \mathcal{E}}{2} \quad ; \quad d_2 = \mathcal{B} + \mathcal{E}, \quad (23)$$



where we defined two new constants  $\mathcal{B}$  and  $\mathcal{E}$  as

$$\mathcal{B} = \frac{a_e^4 \mathcal{P}_B^{\text{inf}}(\eta_{\text{end}})}{f^2(\eta_{\text{end}})} = \frac{k^4}{8\pi} \frac{2^{2n+1} \Gamma^2(n + \frac{1}{2})}{\pi^2} \left(\frac{k}{k_e}\right)^{-2n}, \quad (24)$$

$$\mathcal{E} = \frac{a_e^4 \mathcal{P}_E^{\text{inf}}(\eta_{\text{end}})}{f^2(\eta_{\text{end}})} = \frac{k^4}{8\pi} \frac{\Gamma^2(n - \frac{1}{2}) 2^{2n-1}}{\pi^2} \left(\frac{k}{k_e}\right)^{2-2n} \quad (25)$$

In de Sitter space, we can identify it through  $|\eta_{\text{end}}| = 1/k_e$  where  $k_e$  is the highest model that crossed the horizon at the end of inflation. The above two Eqs. (24),(25) are evaluated at the end of inflation for the super-horizon modes approximation.

Many existing cosmological magnetogenesis models assume that, following inflation, fields on super-horizon scales experience a radiation-like redshift, with the magnetic energy density scaling as  $\rho_{\text{em}} \propto a^{-4}$  [36–40, 76]. However, it is important to note that the individual evolution of the electric and magnetic field components,  $E^2$  and  $B^2$ , may deviate from this assumption, as their behavior depends sensitively on the conductivity of the universe during reheating [35, 77, 78]. This nontrivial evolution can be attributed to Faraday induction, through which electric energy can be converted into magnetic energy, and vice versa, depending on the field strengths [35, 78].

In non-helical magnetogenesis scenarios, it is typically observed that either the magnetic or electric field strength dominates at the end of inflation, as pointed out before about the Eqs. (14) and (15). Due to this hierarchy between the electric and magnetic energy densities, the subsequent evolution is strongly influenced by the conductivity. In cases where the electric field dominates over the magnetic field at the end of inflation (for  $n < -1/2$ ), the electric energy is gradually converted into magnetic energy, thereby amplifying the magnetic field strength [35]. Conversely, when the magnetic field dominates (for  $n > 1/2$ ), energy is transferred from the magnetic field to the electric field.

In the high-conductivity limit, rapid charge separation generates counter-electric fields that effectively cancel the electric component, leaving only the magnetic field. In this case, the magnetic field evolves adiabatically, and its energy density redshifts as  $\rho_B \propto a^{-4}$ . Although our primary interest lies in modes that are far outside the horizon at the end of reheating, the role of conductivity for such superhorizon modes remains subtle. Conductivity arises in a causal process; however, for the super-horizon modes, causality prevents different regions from communicating, raising the possibility that these large-scale modes might not “feel” the effects of high conductivity, even though the universe as a whole is highly conductive. If these modes indeed remain unaffected by conductivity, the dynamics involving energy conversion between the electric and magnetic fields would still apply during reheating. But for this paper, we simply consider two limiting scenarios in our analysis: one with zero electrical conductivity and another with infinite electrical conductivity during the reheating phase.

*a. The case of negligible conductivity during reheating* If we assume zero electrical conductivity in the universe during the reheating period, both electric and magnetic fields are present, with the strength of the fields depending on their coupling to the background. As shown in Eqs.(16) and (17), for  $n > 1/2$ , we obtain a stronger magnetic field, and for  $n < -1/2$ , the electric field’s strength is dominant over the magnetic field at early stages. We consider both scenarios, and their evolution during reheating is governed by the following.

$\mathcal{P}_B \gg \mathcal{P}_E$ : The modes of interest in this context have a scale of approximately  $1 \text{ Mpc}^{-1}$ , which is well outside the Hubble radius at the end of reheating. Therefore, we can consider the limit where  $k(\eta - \eta_{\text{end}}) \ll 1$ , and in this limit, the equations (22a) simplify to:

$$a_{\text{re}}^4 \mathcal{P}_B(k, \eta_{\text{re}}) \simeq \mathcal{B} - (\mathcal{B} - \mathcal{E}) k^2 \eta_{\text{re}}^2 \quad (26)$$

$$a_{\text{re}}^4 \mathcal{P}_E(k, \eta_{\text{re}}) \simeq \mathcal{E} + (\mathcal{B} - \mathcal{E}) k^2 \eta_{\text{re}}^2 \quad (27)$$

It is worth noting that for positive values of  $n$ , the magnetic field is stronger than the electric field, as indicated in Eq. (16). Furthermore, from Eqs. (24) and (25), it is evident that  $\mathcal{B} \gg \mathcal{E}$ . As demonstrated above, the efficiency of energy transfer from magnetic to electric components is notably sensitive to the duration of the reheating phase. We will explore this dependence in greater detail in a subsequent section.

$\mathcal{P}_E \gg \mathcal{P}_B$ : In a similar manner to what was stated previously, if we take into account the negative value of  $n$ , we observe that the electric field surpasses the magnetic field strength at the end of inflation. Consequently, during reheating on the superhorizon scale limit, the spectrum evolves into,

$$\begin{aligned} a_{\text{re}}^4 \mathcal{P}_E(k, \eta_{\text{re}}) &\simeq \mathcal{B} - (\mathcal{B} - \mathcal{E}) k^2 \eta_{\text{re}}^2 \\ a_{\text{re}}^4 \mathcal{P}_B(k, \eta_{\text{re}}) &\simeq \mathcal{E} + (\mathcal{B} - \mathcal{E}) k^2 \eta_{\text{re}}^2. \end{aligned} \quad (28)$$

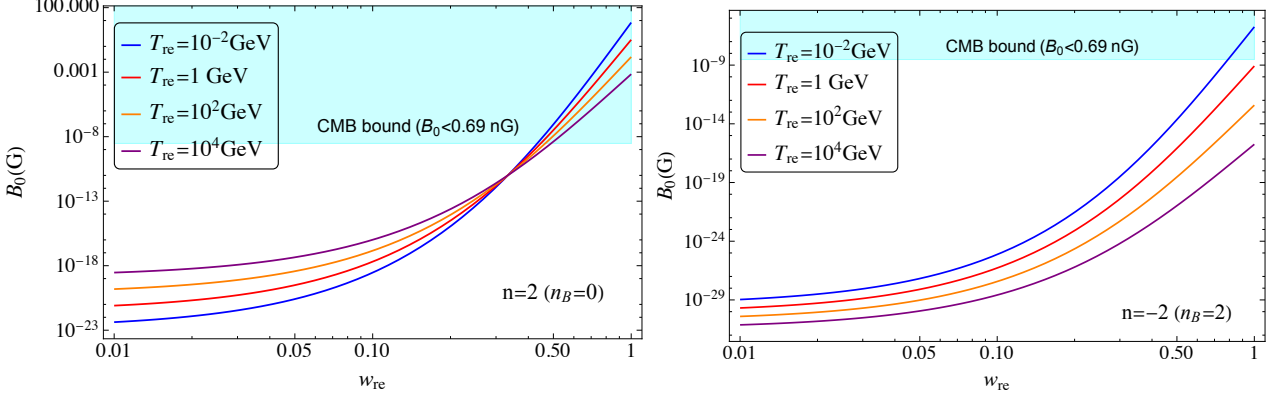


FIG. 1: The figures mentioned above illustrate the present-day magnetic field strength at the 1 Mpc length scale, denoted as  $B_0$  (in Gauss), as a function of the equation of state  $w_{re}$ . Different colors represent various reheating temperatures  $T_{re}$  (in GeV). The right plot is  $n = -2$ , resulting in a pronounced blue-tilted magnetic spectrum ( $n_B = 2$ ). In contrast, the left figure represents the case of  $n = 2$ , yielding a scale-invariant magnetic spectrum with  $n_B = 0$ . In both figures, the cyan-shaded region denotes an excluded area due to the upper limit on the present-day magnetic field strength at the 1 Mpc scale, as derived from constraints imposed by the Cosmic Microwave Background (CMB) [56, 79].

In this instance, we note that the electric field energy density is converted into magnetic field energy density. We have also found that the conversion of the energy density is proportional to the energy difference of the two fields, and it is directly related to the total duration of the reheating periods. It means a longer duration of the reheating periods allows more conversion of the energy density. Effectively, at the super-horizon scale, the strength of the magnetic field also increases significantly. Such a conversion mechanism turns out to be helpful for the  $n < -1/2$  case, when the magnetic field strength at large scale is low at the end of inflation, as it yields a strong magnetic field at present without any strong coupling as well as backreaction issues.

Based on the preceding discussion, it is evident that if we consider zero (or small) conductivity during the reheating phase, the individual components of the electromagnetic field, namely  $B^2$  and  $E^2$ , undergo non-trivial evolution. Moreover, the field strength is directly linked to the reheating parameters, specifically the *reheating temperature*  $T_{re}$  and the average equation of state  $w_{re}$ . If we wish to express how the comoving magnetic field evolves as a function of these reheating parameters, we must carefully account for the energy transfer dynamics between the electric and magnetic components, and we have the following

$$a_{re}^4 \mathcal{P}_B(k, \eta_{re}) = \begin{cases} \mathcal{B} - (\mathcal{B} - \mathcal{E}) \left(\frac{k}{k_e}\right)^2 \text{Exp}[N_{re}(1 + 3w_{re})] & \text{for } n > \frac{1}{2} \\ \mathcal{E} + (\mathcal{B} - \mathcal{E}) \left(\frac{k}{k_e}\right)^2 \text{Exp}[N_{re}(1 + 3w_{re})] & \text{for } n < -\frac{1}{2} \end{cases} \quad (29)$$

Here  $N_{re}$  is the e-folding number of the reheating phase, which can be directly related to the reheating temperature through Eq.(8) [70, 72, 73].

**b. The case of infinite conductivity during reheating:** If we assume an infinite conductivity limit during reheating, the only remaining field is the magnetic field, and its energy density evolution follows the relation  $\rho_{em} = \rho_B \propto a^{-4}$ . The energy density dilutes due to the expansion of the universe, and the comoving magnetic power spectrum freezes after inflation ends as any conversion or production ceases to exist during this period. Thus, at the superhorizon scale, after the end of reheating, the magnetic power spectrum is defined as

$$\begin{aligned} a_{re}^4 \mathcal{P}_B(k, \eta_{re}) &= \frac{k^4}{8\pi} \frac{2^{2n+1} \Gamma^2(n + \frac{1}{2})}{\pi^2} \left(\frac{k}{k_f}\right)^{-2n} & \text{for } n > \frac{1}{2} \\ a_{re}^4 \mathcal{P}_B(k, \eta_{re}) &= \frac{k^4}{8\pi} \frac{2^{2n-1} \Gamma^2(n - \frac{1}{2})}{\pi^2} \left(\frac{k}{k_f}\right)^{2-2n} & \text{for } n < -\frac{1}{2} \end{aligned} \quad (30)$$

**c. Constraining Parameters from CMB Temperature Fluctuations ( $\delta T/T \simeq 10^{-5}$ ):** The evolution of the universe after inflation is critical for determining the present-day magnetic field strength generated during this era. During reheating, the background energy density (inflaton energy density  $\rho_\phi$ ) evolves as  $a^{-3(1+w_{re})}$ . In contrast, the electromagnetic (EM) energy density  $\rho_{em}$  evolves as  $a^{-4}$  due to background expansion.



EqS	$w_{re} = 0.5$				$w_{re} = 0.6$			
$n_B$	0.01	0.2	0.4	0.6	0.01	0.2	0.4	0.6
$T_{re}$ (GeV)	$9.09 \times 10^5$	$1.84 \times 10^3$	215.5	48.9	$1.68 \times 10^9$	$2.7 \times 10^7$	$6.52 \times 10^6$	$2.2 \times 10^6$
$B_0$ (G)	$1.47 \times 10^{-9}$	$1.4 \times 10^{-11}$	$5.0 \times 10^{-14}$	$1.51 \times 10^{-16}$	$1.475 \times 10^{-9}$	$1.407 \times 10^{-11}$	$5.04 \times 10^{-14}$	$1.56 \times 10^{-16}$

TABLE I: Upper bounds on reheating temperature consistent with CMB temperature fluctuations (Eq. (31)) and the corresponding present-day magnetic field strength  $B_0$  in Gauss.

sion. Thus, the EM energy density fluctuation  $\delta_{EM} = \rho_{EM}/\rho_\phi$  scales as  $\delta_{EM} \propto a^{(3w_{re}-1)}$ , making it sensitive to both the fluid's nature (defined by  $w_{re}$ ) and the reheating duration (set by the reheating temperature  $T_{re}$ ).

To align with CMB observations, the temperature fluctuations should satisfy  $\delta T/T \leq 10^{-5}$ . Assuming all temperature fluctuations arise from the EM energy density (although this is a very crude approximation), the EM energy density at the end of reheating must adhere to this constraint. Due to high conductivity following reheating, any electric field dissipates quickly, leaving only the magnetic component relevant when  $n > 1/2$  (where  $n$  is the coupling constant). This analysis excludes MHD effects, which are significant only for sub-horizon modes and may have changed the bounds.

Based on these considerations, we derive the constraint:

$$\frac{2^{2n+1}\Gamma^2(n+1/2)}{24\pi^3(4-2n)} \left(\frac{H_1}{M_P}\right)^2 \left\{1 - \left(\frac{k_*}{k_e}\right)^{4-2n}\right\} \left(\frac{a_e}{a_{re}}\right)^{1-3w_{re}} \leq 4\frac{\delta T}{T}, \quad (31)$$

where this bound is effective only for  $w_{re} > 1/3$  due the factor  $(a_e/a_{re})^{1-3w_{re}}$ . From this, we constrain the reheating dynamics and determine the maximum possible present-day magnetic field strength, denoted  $B_0$ .

In Table (I), we present the lower bounds on the reheating temperature for  $w_{re} = 0.5$  and  $w_{re} = 0.6$ , across various values of the magnetic spectral index  $n_B = 4 - 2n$ . We also provide the corresponding present-day magnetic field strength in Gauss, defined at a scale of  $1 \text{ Mpc}^{-1}$ . These bounds are derived under certain assumptions discussed earlier.

In particular, we neglect the magnetohydrodynamic (MHD) evolution of sub-horizon modes, which are most significantly affected by MHD processes. Therefore, for blue-tilted magnetic spectra, the results presented here are expected to be substantially modified in a more realistic scenario. However, since a full treatment of MHD dynamics is beyond the scope of this work, we present these bounds as indicative estimates.

For instance, considering a nearly scale-invariant spectrum with  $n_B = 0.01$ , we find that for  $w_{re} = 0.5$ , the minimum reheating temperature is approximately  $T_{re} \simeq 9.09 \times 10^5 \text{ GeV}$ , with a corresponding present-day magnetic field strength of  $B_0 \simeq 1.47 \times 10^{-9} \text{ G}$  at  $1 \text{ Mpc}$ . For  $w_{re} = 0.6$ , the reheating temperature increases to  $T_{re} \simeq 1.68 \times 10^9 \text{ GeV}$ , with a similar magnetic field strength of  $B_0 \simeq 1.475 \times 10^{-9} \text{ G}$ . Results for other values of  $w_{re}$  and  $n_B$  are summarized in Table (I).

In Fig. (1), we depict the strength of the present-day magnetic field  $B_0$  as a function of the equation of state  $w_{re}$ , with  $w_{re}$  ranging from 0 to 1. Four different colors represent four distinct reheating temperatures. In the left plot, we assume a specific coupling  $n = 2$ , which yields a scale-invariant magnetic spectrum, while the electric spectrum scales as  $\mathcal{P}_E \propto k^2$ . Depending on the duration of reheating, a significant conversion of energy occurs from the magnetic field to the electric field ( $\rho_B \rightarrow \rho_E$ ). However, for this particular coupling ( $n = 2$ ), the comoving magnetic energy density remains conserved on large scales.

We observe that as the equation of state increases, the present-day magnetic field strength also gradually increases. This is due to the rate of dilution: when  $w_{re} > 1/3$ , the background energy density dilutes faster than the radiation energy density, and the universe spends less time in reheating compared to scenarios with  $w_{re} < 1/3$ . Hence, the relative dilution of the magnetic field compared to the background is diminished, causing the effective present-day magnetic field strength to be larger for a higher equation of state.

For a scale-invariant magnetic spectrum ( $n_B = 0$ ), the maximum allowed equation of state (EqS) parameter during reheating is approximately  $w_{re} \simeq 0.5$  across a wide range of reheating temperatures, as illustrated in Fig. 1. Higher values of  $w_{re}$  are disfavoured, as they lead to magnetic field strengths at the  $1 \text{ Mpc}^{-1}$  scale that exceed the current upper limits set by CMB observations. In contrast, for a blue-tilted magnetic spectrum, this constraint is significantly relaxed, as shown in the right panel of Fig. 1.

In the right panel, we plot  $B_0$  against  $w_{re}$  for different reheating temperatures  $T_{re}$ , considering a different coupling relationship ( $n = -2$ ), which results in a scale-dependent magnetic field. In this case, the magnetic power spectrum follows a  $\mathcal{P}_B(k, \eta_0) \propto k^2$  behavior, leading to a stronger electric field compared to the magnetic field. In the absence of electrical conductivity, we observe significant energy conversion from the electric field to the magnetic field, with the extent of conversion depending on the duration of reheating.

Lowering the reheating temperature increases the duration of the reheating phase, allowing greater energy transfer and leading to higher magnetic field strengths. Interestingly, we find that inflationary production alone, without prolonged reheating, is insufficient to generate magnetic fields strong enough to match present-day observations for coupling types with  $n < -1/2$ .

However, when prolonged reheating with negligible electrical conductivity is considered, efficient energy transfer from the electric to the magnetic field becomes possible, thereby enhancing the magnetic field strength to observationally viable levels. For example, with  $w_{re} = 0.5$  and  $T_{re} \sim 10^{-2}$  GeV, even for couplings with  $n < -1/2$ , the magnetic field strength at 1 Mpc can reach up to  $B_0 \sim 10^{-14}$  G, which lies well within the current observational bounds.

In contrast, if we impose the CMB constraints on temperature fluctuations discussed above, then for  $w_{re} = 0.5$ , the lowest allowed reheating temperature is  $T_{re} \sim 9.1 \times 10^5$  GeV. In this case, the corresponding present-day magnetic field strength is  $B_0 \sim 6.4 \times 10^{-23}$  G, which is about  $10^{12}$  times larger than the scenarios where we have no such conversion of the energy from electric field to magnetic field. In radiation-like reheating scenarios with negligible electrical conductivity, for a reheating temperature of  $T_{re} = 10^{-2}$  GeV, the maximum possible conversion of electric field energy into magnetic field energy is allowed. In this case, we find that the present-day magnetic field strength can reach up to  $B_0 \sim 2.6 \times 10^{-18}$  G.

On the other hand, for matter-like reheating scenarios ( $w_{re} = 0$ ) with the same reheating temperature  $T_{re} = 10^{-2}$  GeV, even after significant conversion from electric to magnetic fields, the present-day magnetic field strength is much lower, approximately  $B_0 \sim 3.7 \times 10^{-30}$  G. Although a matter-like reheating phase leads to a longer reheating duration, allowing more efficient conversion of electric energy into magnetic energy, the extended post-inflationary expansion results in greater dilution of the magnetic energy density, causing the present-day magnetic field strength to be significantly lower despite the effective energy transfer.

Thus, the post-inflationary evolution of the gauge field plays a crucial role in determining the present-day magnetic field strength. Furthermore, the electrical conductivity of the Universe during reheating significantly influences the final magnetic field amplitude.

### III. GENERATION OF GRAVITATIONAL WAVES:

The early universe provides a rich setting for gravitational wave (GW) generation, with primary contributions from quantum fluctuations during inflation and secondary sources such as primordial electromagnetic (EM) fields. Quantum fluctuations in spacetime, amplified during inflation, imprint a stochastic GW background that carries signatures of the inflationary dynamics. However, beyond this primary GW production, secondary sources—particularly EM fields—can significantly enhance the GW spectrum. Magnetic and electric fields, likely generated through the above-mentioned process, can further enrich the GW signal and offer new observational windows into early universe physics. In this section, we mainly explore the secondary contributions from EM fields, highlighting their distinct and complementary roles in shaping the detectable GW landscape.

The GW perturbed Friedmann-Robertson-Walker (FRW) metric takes the form:

$$ds^2 = a^2(\eta) (-d\eta^2 + (\delta_{ij} + h_{ij})dx^i dx^j), \quad (32)$$

where ‘ $\eta$ ’ is the conformal time and  $h_{ij}$  is the traceless tensor, i.e.,  $\partial^i h_{ij} = h_i^i = 0$ . In Fourier space, the equation of motion for the gravitational wave amplitude ‘ $h$ ’, for either polarization  $h^+$  or  $h^-$ , becomes [15–20]:

$$h_{\mathbf{k}}'' + 2\mathcal{H}h_{\mathbf{k}}' + k^2 h_{\mathbf{k}} = \mathcal{S}(\mathbf{k}, \eta), \quad (33)$$

where  $\mathcal{S}$  is the source term. Here we consider electromagnetic fields as the source term, which can be written as

$$\mathcal{S}_\lambda(\mathbf{k}, \eta) = -\frac{f^2(\eta)}{a^2(\eta)} \int \frac{d^3 q}{(2\pi)^{3/2}} e_\lambda^{ij}(\mathbf{k}) \{ A_i'(\mathbf{q}, \eta) A_j'(|\mathbf{k} - \mathbf{q}|, \eta) - \epsilon^{iab} q_a A_b(\mathbf{q}, \eta) \epsilon^{icd} (k - q)_c A_d(|\mathbf{k} - \mathbf{q}|, \eta) + \dots \}. \quad (34)$$

In the above, we consider only those relevant terms contributing to tensor production. Here  $e_{\lambda}^{ij}(\mathbf{k})$  is the polarization tensor, and for a non-helical magnetic field, it is convenient to choose a linear polarization basis defined as  $e_{ij}^{\pm} = \frac{1}{\sqrt{2}}(\hat{e}_1 \times \hat{e}_2 \pm \hat{e}_2 \times \hat{e}_1)_{ij}$ , which satisfies  $\delta_{ij}e_{\lambda}^{ij}(\mathbf{k}) = \mathbf{k}_i e_{\lambda}^{ij}(\mathbf{k}) = 0$  and  $e_{il}^{\lambda}(\mathbf{k})e_{lj}^{\lambda}(-\mathbf{k}) = \delta_{ij}$ . Here  $\hat{e}_1$  &  $\hat{e}_2$  are a set of mutually orthonormal basis vectors of our coordinate system. The inhomogeneous solution of Eq. (33) can then be written as

$$h_{\mathbf{k}}(\eta) = \int_{\eta_i}^{\eta} d\tilde{\eta} \mathcal{G}_{\mathbf{k}}(\eta, \tilde{\eta}) \mathcal{S}(\mathbf{k}, \tilde{\eta}), \quad (35)$$

where  $\mathcal{G}_{\mathbf{k}}$  is the Green's function of associated operator of Eq. (33). The GW spectrum is defined as

$$\langle h_{\mathbf{k}}^{(\lambda)} h_{\mathbf{k}'}^{(\lambda)} \rangle = \frac{2\pi^3}{k^3} \mathcal{P}^{(\lambda)}(k, \eta) \delta^{(3)}(\mathbf{k} + \mathbf{k}'). \quad (36)$$

It is convenient to express the tensor power spectrum as the sum of two components: one arising from vacuum fluctuations and the other from source terms. These two contributions are uncorrelated, so we write them as:

$$\mathcal{P}^{\lambda}(k, \eta) = \mathcal{P}_{\text{PRI}}^{\lambda}(k, \eta) + \mathcal{P}_{\text{SEC}}^{\lambda}(k, \eta), \quad (37)$$

where  $\mathcal{P}_{\text{PRI}}^{\lambda}(k, \eta)$  refers to vacuum production, and  $\mathcal{P}_{\text{SEC}}^{\lambda}(k, \eta)$  is due to the EM field. For a general case with a power-law type electromagnetic spectrum  $\mathcal{P}_{\text{B/E}}(k, \eta) \propto (k\eta)^{n_{\text{B/E}}}$ , the tensor power spectrum at any time  $\eta$  can be written as [28]

$$\mathcal{P}_{\text{SEC}}^{\lambda}(k, \eta) = \frac{2}{M_{\text{P}}^4} \left[ \int_{\eta_i}^{\eta} d\eta_1 a^2(\eta_1) \mathcal{G}_k(\eta_f, \eta_1) \mathcal{P}_{\text{B/E}}(k, \eta_1) \right]^2 \times \int_0^{\infty} \frac{dq}{q} \int_{-1}^1 d\mu \frac{(q/k)^{n_{\text{B/E}}} f(\mu, \beta, \lambda)}{\left[ 1 + \left(\frac{q}{k}\right)^2 - 2\mu \frac{q}{k} \right]^{\frac{3-n_{\text{B/E}}}{2}}} \quad (38)$$

where  $f(k, q, \lambda) = (1 + \mu^2)(1 + \beta^2)$ , with  $\mu = \hat{\mathbf{k}} \cdot \hat{\mathbf{q}}$  and  $\beta = \widehat{\mathbf{k} - \mathbf{q}} \cdot \hat{\mathbf{k}}$  [19, 28, 56, 80]. Here,  $n_{\text{B/E}}$  is the spectral index for the magnetic or electric field, depending on which field dominates during this era.

### A. Generation and Evolution of Primary Gravitational Waves

Considering a well-known slow-roll inflation scenario, approximated by a de Sitter universe with the scale factor evolving as  $a(\eta) = (1 - H_1 \eta)^{-1}$ , where  $H_1$  represents the Hubble constant during inflation. Where the homogeneous solution of Eq. (33), with Bunch-Davies initial conditions, is given by [14]

$$h_{\mathbf{k}}(\eta) = \frac{\sqrt{2}}{M_{\text{P}}} \frac{iH_1}{\sqrt{2}k^3} \left[ 1 - \frac{ik}{H_1 a(\eta)} \right] e^{-ik/H_1} e^{ik/(H_1 a(\eta))}. \quad (39)$$

This demonstrates that the amplitude of the tensor fluctuations is directly related to the energy scale of inflation, i.e.,  $h_{\mathbf{k}} \propto H_1$ . At the end of inflation ( $\eta = \eta_e$ ), we can define the tensor power spectrum as [11–14]

$$\mathcal{P}_{\text{inf}}^{\text{PRI}}(k) = \frac{2}{\pi^2} \left( \frac{H_1}{M_{\text{P}}} \right)^2 \left( 1 + \frac{k^2}{k_e^2} \right), \quad (40)$$

where  $k_e$  is the highest mode that exited the horizon during inflation.

After inflation, the universe undergoes different phases, and the initial fluctuations are modified as they pass through these phases, encoding information about the universe's history. We consider a non-instantaneous reheating scenario, where the scale factor evolves as  $a(\eta) \simeq a_e (\eta/\eta_e)^{\delta/2}$ , with  $\delta = 4/(1 + 3w_{re})$ , where  $w_{re}$  is the average equation of state (EoS) during reheating. Solving the homogeneous part of Eq. (33) during the reheating phase, the tensor fluctuations  $h_{\mathbf{k}}$  in the super-horizon approximation ( $k < k_e$ ) are given by

$$h_{\mathbf{k}}(\eta > \eta_e) \simeq \frac{\pi^2 x^l}{2\Gamma(l)\Gamma(1-l)} \left[ \frac{2-l}{\Gamma(2-l)} \left( \frac{k}{k_e} \right)^{2(1-l)} J_l(x) + \frac{1}{\Gamma(l)} J_{-l}(x) \right] h_{\mathbf{k}}(\eta_e), \quad (41)$$

where  $x = k\eta$ ,  $l = 3(w_{re} - 1)/2(1 + 3w_{re})$  and  $J_l(x)$  is The Bessel functions of the first kind. Here,  $h_{\mathbf{k}}(\eta_e)$  is the tensor fluctuation produced during inflation, defined at the end of inflation, and includes contributions from both quantum fluctuations and source terms, such as EM fields.

After reheating, the universe enters a radiation-dominated phase, where the background energy density scales as  $a^{-4}$  due to expansion. During this phase, the scale factor evolves as  $a(\eta) \propto \eta$ . Solving the homogeneous part of Eq. (33) in this era, the tensor fluctuation  $h_{\mathbf{k}}(\eta > \eta_{re})$  takes the form

$$h_{\mathbf{k}}(\eta > \eta_{re}) = x^{-1} (\mathcal{D}_1 e^{-ix} + \mathcal{D}_2 e^{ix}), \quad (42)$$

where  $\mathcal{D}_1$  and  $\mathcal{D}_2$  are constants defined by

$$\mathcal{D}_1(x_{re}) = \frac{h_{\mathbf{k},re}^\lambda(x_{re})(ix_{re} - 1) - x_{re}h_{\mathbf{k},re}^{\lambda'}(x_{re})}{2i} e^{ix_{re}}, \quad (43a)$$

$$\mathcal{D}_2(x_{re}) = \frac{x_{re}h_{\mathbf{k},re}^{\lambda'}(x_{re}) + h_{\mathbf{k},re}^\lambda(x_{re})(ix_{re} + 1)}{2i} e^{-ix_{re}}. \quad (43b)$$

Here  $h_{\mathbf{k},re}^\lambda$  and  $h_{\mathbf{k},re}^{\lambda'}$  are the defined tensor fluctuations and their 1st derivative at the end of reheating. It contains both the inflationary effects of the primary production and secondary production of the tensor perturbation. Using Eq. (43), we define the tensor power spectrum during the radiation-dominated era (due to the homogeneous solution of the tensor equation) as

$$\mathcal{P}(k, \eta > \eta_{re}) \simeq \frac{1}{2(k\eta)^2} \left( 1 + \left( \frac{k}{k_{re}} \right)^2 \right) \mathcal{P}(k, \eta_{re}). \quad (44)$$

Here,  $\mathcal{P}(k, \eta_{re})$  represents the total tensor power spectrum at the end of reheating. For modes that remain outside the horizon at the end of reheating ( $k < k_{re}$ ), the tensor power spectrum in the radiation-dominated era scales proportionally to the inflationary tensor power spectrum, i.e.,  $\mathcal{P}(k, \eta > \eta_{re}) \propto \mathcal{P}(k, \eta_e)$ . However, for modes that re-entered the horizon before reheating ended ( $k > k_{re}$ ), the tensor power spectrum is affected by the reheating history, scaling as  $\mathcal{P}(k > k_{re}) \propto x_{re}^{2l+1} \mathcal{P}(k, \eta_e)$ , where  $x_{re} = k\eta_{re}$ .

## B. Generation of Secondary Gravitational Waves

Electromagnetic (EM) fields in the early universe offer a compelling secondary source of gravitational waves (GWs), capable of amplifying the GW spectrum beyond inflationary contributions. There are three different phases where we can expect that the Electromagnetic field can have the potential to generate the GW signal enough that it can be passed through different future observatories. We consider that electromagnetic fields are generated during inflation (discussed in sec.(II)), which has significant strength (depending on the model parameters). The electromagnetic fields are one of the key sources that can generate gravitational waves during inflation as well as the post-inflationary era. Now, to see the contributions due to the EM field during inflation, we are going to use the Green's function method like [28]. During inflation in a de Sitter background, the Green's function is well established [81],

$$\mathcal{G}_k^{\text{inf}}(\eta, \eta') = \frac{1}{k^3 \eta'^2} [(1 + k^2 \eta \eta') \sin(k(\eta - \eta')) + k(\eta' - \eta) \cos(k(\eta' - \eta))] \Theta(\eta - \eta'). \quad (45)$$

Assuming that at the end of inflation  $\eta \rightarrow 0$ , the Green's function simplifies, and we can write it as

$$\mathcal{G}_k^{\text{inf}}(0, \eta') = \frac{1}{k^3 \eta'^2} [-\sin(k\eta') + k\eta \cos(k\eta')]. \quad (46)$$

It is evident that the primary contribution to Green's function arises from the superhorizon scale, particularly in the limit  $|k\eta'| \ll 1$ . In this regime, we can approximate  $\mathcal{G}_k(\eta') \approx \eta'/3$ . Utilizing these considerations and incorporating all assumptions, we proceed to derive the tensor power spectrum after inflation within the de Sitter inflationary background

$$\mathcal{P}_{T,s}^{\text{inf}}(k, \eta_e) = 2 \left( \frac{H_1}{M_{\text{Pl}}} \right)^4 \mathcal{C}_{\text{B/E}}^2(n_{\text{B/E}}) \left( \frac{k}{k_e} \right)^{2n_{\text{B/E}}} \mathcal{I}_{\text{inf}}^2 \mathcal{F}_{n_{\text{B/E}}}(k), \quad (47)$$

where  $\mathcal{I}_{\text{inf}} = (1 - (k_e/k_{\text{min}})^{n_{\text{B/E}}})/3n_{\text{B/E}}$  and we also define,

$$\mathcal{C}_{\text{B/E}}(n_{\text{B/E}}) = \frac{2^{5-n_{\text{B/E}}} \Gamma^2\left(\frac{5-n_{\text{B/E}}}{2}\right)}{8\pi^3} \quad (48)$$

and

$$\mathcal{F}_{n_{\text{B/E}}}(k) = \frac{8}{3n_{\text{B/E}}} \left(1 - \left(\frac{k_{\text{min}}}{k}\right)^{n_{\text{B/E}}}\right) + \frac{56}{15(2n_{\text{B/E}} - 3)} \left(\left(\frac{k_e}{k}\right)^{2n_{\text{B/E}}-3} - 1\right). \quad (49)$$

Here  $k_{\text{min}}$  is the lowest possible scale. As in this case we consider a non-helical magnetogenesis model discussed in sec.(II), depending on the nature of the coupling, one of the fields, either the magnetic field or the electric field, is the dominating component. So, if we change the nature of the coupling, the final spectrum behavior will also change. But at the end of inflation, it is very hard to distinguish, as for this type of coupling we have the same behavior when we change the sign of the coupling constant  $n$  (see in Eqs. (16)(17)). However, when the universe evolves through different phases, there will be a significant change in the overall GW spectrum at present, which will be discussed in detail later. But at the end of inflation, we have found that at large scales, such as those associated with the CMB, the primary production is more dominant compared to the secondary as  $\mathcal{P}_{\text{V}}^{\text{inf}}(k) \propto (H_1/M_{\text{P}})^2$ , whereas  $\mathcal{P}_{\text{S}}^{\text{inf}}(k) \propto (H_1/M_{\text{P}})^4$ , where  $\mathcal{P}_{\text{V}}^{\text{inf}}(k)$  is the contribution due to quantum fluctuations and  $\mathcal{P}_{\text{S}}^{\text{inf}}(k)$  is the contribution due to EM fields.

After inflation, we have the reheating phase, where all the fundamental particles are produced. Depending on the conductivity during this time, the nature of the GWs produced due to EM fields also changes. Here, we consider two extreme scenarios: either we consider that during the reheating phase the effective conductivity of our universe is very low (for simplicity, we consider zero conductivity), or we can consider that initial production of charge particles were enough that during this phase the conductivity was very high (for simplicity, we consider infinite conductivity scenario). When we consider zero electric conductivity, both the electric and magnetic fields contribute, whereas in the other case, electric fields vanish, and only the magnetic field contributes to secondary gravitational waves. During the reheating phase, the Green's function can be written as [28],

$$\mathcal{G}_{\mathbf{k}}(x, x_1) = \theta(x - x_1) \frac{\pi x^l x_1^{1-l}}{2k \sin(l\pi)} [J_l(x) J_{-l}(x_1) - J_{-l}(x) J_l(x_1)] \quad (50)$$

In general, we can define the tensor power spectrum generated during reheating due to the EM field, as defined at the end of reheating, by the following expression

$$\mathcal{P}_{T,s}^{\text{re}} = \frac{2H_1^4}{M_{\text{P}}^4} \left(\frac{k}{k_e}\right)^{2(\delta-2)} \mathcal{C}_{\text{B/E}}^2(n_{\text{B/E}}) \left(\frac{k}{k_e}\right)^{2n_{\text{B/E}}} \mathcal{C}_{\text{m, re}}^2(x_{\text{re}}, x_{\text{end}}) \mathcal{F}_{n_{\text{B/E}}}(k), \quad (51)$$

where  $\mathcal{F}_{n_{\text{B/E}}}$  is defined in Eq. (49) and  $\mathcal{C}_{\text{m, re}}(x_{\text{re}}, x_{\text{end}})$  is defined as [28]

$$\mathcal{C}_{\text{m, re}}(x_{\text{re}}, x_{\text{end}}) = \int_{x_{\text{end}}}^{x_{\text{re}}} dx_1 x_1^{-\delta} \mathcal{G}_{\mathbf{k}}(x_{\text{re}}, x_1), \quad (52)$$

If we analyze the spectrum, we find that due to the non-instantaneous reheating phase, the overall spectrum has a term like  $(k_{\text{re}}/k_e)^{2(\delta-2)}$ . We recall that  $\delta = 4/(1 + 3w_{\text{re}})$ . So, depending on the nature of the reheating scenarios, either the overall spectrum gets enhanced (for  $w_{\text{re}} > 1/3$ ) or suppressed (for  $w_{\text{re}} < 1/3$ ). Although we have also found that for those modes which are outside the horizon  $k < k_{\text{re}}$ , the secondary spectrum always goes as  $\mathcal{P}_{\text{S}}^{\text{re}}(k \ll k_{\text{re}}, \eta_{\text{re}}) \propto k^{2n_{\text{B/E}}}$ , whereas for those modes which are inside the horizon, it goes as  $\mathcal{P}_{\text{S}}^{\text{re}}(k \gg k_{\text{re}}, \eta_{\text{re}}) \propto k^{2n_{\text{B/E}} - |n_w| - 2}$ . Here,  $n_w = 2(1 - 3w_{\text{re}})/(1 + 3w_{\text{re}})$ .

During the radiation-dominated era, the electrical conductivity of our universe was very high, and the only existing component was the magnetic field, which produces GWs. It is well known that such production is only effective up to the neutrino decoupling era. After neutrinos decouple from the thermal bath, they effectively cancel the anisotropy due to magnetic fields [82].

Thus, the tensor power spectrum due to the magnetic field after reheating, defined at the time of neutrino decoupling, is governed by the expression [28]

$$\mathcal{P}_{\text{ra, SEC}}^{\lambda}(k, \eta_{\nu}) = \frac{2H_1^4}{k^2 \eta_{\nu}^2 M_{\text{P}}^4} \left(\frac{k_{\text{re}}}{k_e}\right)^{2(\delta-2)} \mathcal{C}_{\text{B/E}}^2(n_{\text{B}}) \left(\frac{k}{k_e}\right)^{2(4-|2n|)} \mathcal{I}_{\text{ra}}^2(x_{\nu}, x_{\text{re}}) \mathcal{F}_{n_{\text{B}}}(k) \quad (53)$$

Here,  $\mathcal{I}_{\text{ra}}(x_\nu, x_{re})$  is defined as [28]

$$\mathcal{I}_{\text{ra}}(x_\nu, x_{re}) = \int_{x_{re}}^{x_\nu} dx_1 \frac{\sin(x_1 - x)}{x}. \quad (54)$$

As for the low-frequency regions, we found that  $\mathcal{I}_{\text{ra}} = \gamma_1$ , where  $\gamma_1 \sim 0.5$  at the epoch of neutrino decoupling.

Here, we have seen that there is an overall enhancement factor associated with the tensor power spectrum produced during this phase. This extra enhancement factor comes from the phase of reheating, as during reheating the background energy density dilutes as  $a^{-3(1+w_{re})}$ , whereas the magnetic field always decays as  $a^{-4}$ . Depending on the EoS, where we have  $w_{re} < 1/3$  or  $w_{re} > 1/3$ , the contribution can either be suppressed or enhanced. In this specific kind of magnetogenesis model, we get the effective contribution in the frequency range  $f_\nu < f < f_{re}$  only if we consider  $w_{re} > 1/3$  with  $n > 1/2$ . We recall that here,  $n$  is the coupling constant associated with the magnetogenesis model that we discussed in Sec. (II).

### C. Calculation of the Dimensionless GWs energy density at present time:

During reheating and the radiation-dominated epoch, perturbations re-enter the Hubble radius, generating a stochastic gravitational wave (GW) background. This GW signal, assumed homogeneous, isotropic, and Gaussian, reflects the properties of the FLRW universe. The tensor power spectrum,  $\mathcal{P}^\lambda(k, \eta)$ , a dimensionless quantity dependent on the comoving wavenumber  $k$  and conformal time  $\eta$ , characterizes this background.

Due to the weak gravitational interaction with matter, GWs decouple on Planck scales, allowing us to neglect matter interactions and self-interactions as sub-Hubble GWs propagate freely post-production. The GW energy density, which scales as  $\rho_{\text{GW}} \propto a^{-4}$ , can be normalized by the total energy density at production time,  $\rho_c(\eta)$ . Presently, this density parameter is

$$\Omega_{\text{gw}}(k, \eta) = \frac{\rho_{\text{GW}}(k, \eta)}{\rho_c(\eta)} = \frac{1}{12} \frac{k^2 \mathcal{P}^\lambda(k, \eta)}{a^2(\eta) H^2(\eta)} \quad (55)$$

where  $\rho_c(\eta) = 3H^2(\eta)M_{\text{P}}^2$ , with the reduced Planck mass  $M_{\text{P}} \approx 2.43 \times 10^{18}$  GeV.

The GW energy density follows the radiation scaling behavior, making modes within the Hubble radius near radiation-matter equality particularly relevant. The present-day energy density parameter  $\Omega_{\text{gw}}(k)h^2$  is then given by

$$\Omega_{\text{gw}}(k)h^2 \simeq \left( \frac{g_{*,0}}{g_{*,\text{re}}} \right)^{1/3} \Omega_R h^2 \Omega_{\text{gw}}(k, \eta), \quad (56)$$

where  $\Omega_R h^2 = 4.3 \times 10^{-5}$ ,  $g_{*,\text{re}} = 106.7$ , and  $g_{*,0} = 3.35$  denote relativistic degrees of freedom at the end of reheating and today, respectively.

For simplicity, we decompose the total dimensionless energy density associated with gravitational waves (GWs) into two distinct components, denoted as  $\Omega_{\text{gw}}(k) = \Omega_{\text{gw}}^{\text{pri}}(k) + \Omega_{\text{gw}}^{\text{sec}}(k)$ . Specifically,  $\Omega_{\text{gw}}^{\text{pri}}(k)$  represents contributions originating from quantum vacuum fluctuations, while  $\Omega_{\text{gw}}^{\text{sec}}(k)$  encompasses the contributions attributed to electromagnetic fields. To comprehensively examine the spectral characteristics of GWs across the entire observable frequency spectrum, we separately discuss two distinct scenarios based on the reheating dynamics, namely,  $w_{re} < 1/3$  and  $w_{re} > 1/3$ .

#### 1. Spectral Analysis of Primary Gravitational Waves (PGWs)

Primary Gravitational Waves (PGWs) refer exclusively to the contributions arising from quantum fluctuations during inflation. To analyze the effects of post-inflationary dynamics on the gravitational wave (GW) spectrum, we consider two distinct regimes: (a) super-horizon scales,  $k < k_{\text{re}}$ , where modes remain outside the horizon before the end of reheating, and (b) sub-horizon scales,  $k_{\text{re}} < k < k_{\text{e}}$ , where modes re-enter the horizon before the end of reheating. While inflation alone typically generates a scale-invariant tensor power spectrum, these regimes reveal distinct spectral behaviors. The present-day GW spectrum, produced by inflation, can be expressed as [28, 75]

$$\Omega_{\text{gw}}^{\text{pri}}(k) \simeq 1.12 \cdot 10^{-17} \left( \frac{\Omega_R h^2}{4.3 \cdot 10^{-5}} \right) \left( \frac{H_{\text{I}}}{10^{-5} M_{\text{P}}} \right)^2 \times \begin{cases} 1 & k < k_{\text{re}} \\ (k/k_{\text{re}})^{-n_w} & k_{\text{re}} < k < k_{\text{e}}, \end{cases} \quad (57)$$



From this expression, we observe that, for super-horizon modes ( $k < k_{\text{re}}$ ), the spectrum remains scale-invariant, consistent with the inflationary tensor power spectrum. However, for modes that re-entered the horizon before reheating completed ( $k > k_{\text{re}}$ ), the spectrum is no longer scale-invariant. Specifically, for reheating scenarios with an equation of state  $w_{\text{re}} > 1/3$  (stiff-fluid-like), the spectrum has a blue tilt, while for  $w_{\text{re}} < 1/3$  it has a red tilt. This difference arises because, in  $w_{\text{re}} < 1/3$  scenarios, GW modes that remain inside the horizon for longer durations experience greater dilution, as the background energy density decays more slowly compared to the GW energy density. Conversely, for  $w_{\text{re}} > 1/3$  scenarios, modes are amplified by spending longer periods within the horizon, due to the faster decay of background energy density relative to GW energy density.

## 2. Spectral Analysis of Secondary Gravitational Waves (SGWs)

In analyzing the spectrum of Secondary Gravitational Waves (SGWs) across a wide frequency range, we focus on contributions from magnetogenesis and ignore the primary inflationary GWs. Depending on the coupling parameter in the magnetogenesis model, either strong magnetic fields (for  $n > 1/2$ ) or strong electric fields (for  $n < -1/2$ ) dominate. Additionally, the final spectral characteristics vary with the level of electrical conductivity, leading us to discuss the scenarios separately.

**a. Zero Electrical Conductivity during the Reheating Era:** Assuming zero electrical conductivity, both electric and magnetic fields are present during reheating. Depending on the coupling nature, SGWs are sourced primarily by electric fields (for  $n < -1/2$ ) or magnetic fields (for  $n > 1/2$ ). In reheating scenarios where  $w_{\text{re}} < 1/3$ , the spectral behavior is similar for both cases (either  $n > 1/2$  or  $n < -1/2$ ), differing only in whether the contribution originates from the magnetic or electric field. The SGW spectrum in this regime is given by [28]

$$\Omega_{\text{gw}}^{\text{sec}}(k)h^2 \simeq 2.26 \times 10^{-26} \left( \frac{\Omega_R h^2}{4.3 \times 10^{-5}} \right) \left( \frac{H_{\text{I}}}{10^{-5} M_{\text{P}}} \right)^4 \left( \frac{k_{\text{re}}}{k_{\text{e}}} \right)^{2n_{\text{B/E}}} \mathcal{I}_{\text{inf}}^2 \mathcal{C}_{\beta}^2(n_{\text{B/E}}) \mathcal{F}_{\beta}(k) \times \begin{cases} \left( \frac{k}{k_{\text{re}}} \right)^{2n_{\text{B/E}}}, & k_* < k < k_{\text{re}}, \\ \left( \frac{k}{k_{\text{re}}} \right)^{2n_{\text{B/E}} - |n_w|}, & k_{\text{re}} < k < k_{\text{e}}. \end{cases} \quad (58)$$

For reheating scenarios with  $w_{\text{re}} > 1/3$ , on the other hand, the final spectrum changes depending on whether  $n > 1/2$  or  $n < -1/2$ . When  $n > 1/2$ , the dominant component is the magnetic field, yielding the spectrum[28]

$$\Omega_{\text{gw,pinf}}^{\text{sec}}(k)h^2 \simeq 2.26 \times 10^{-26} \left( \frac{\Omega_R h^2}{4.3 \times 10^{-5}} \right) \left( \frac{H_{\text{I}}}{10^{-5} M_{\text{P}}} \right)^4 \left( \frac{k_{\text{re}}}{k_{\text{e}}} \right)^{2(n_w + n_{\text{B/E}})} \mathcal{C}_{\beta}^2(n_{\text{B}}) \mathcal{F}_{\beta}(k) \times \begin{cases} \mathcal{A}_1 \left( \frac{k}{k_{\text{re}}} \right)^{2n_{\text{B}}}, & k_* < k < k_{\text{ssb}}, \\ \mathcal{I}_2(k) \left( \frac{k_{\text{re}}}{k_{\nu}} \right)^2 \left( \frac{k}{k_{\text{re}}} \right)^{2n_{\text{B}}+2}, & k_{\text{ssb}} < k < k_{\nu}, \\ \mathcal{I}_2(k) \left( \frac{k}{k_{\text{re}}} \right)^{2n_{\text{B}}}, & k_{\nu} \leq k \leq k_{\text{re}}, \\ \mathcal{A}_2 \left( \frac{k}{k_{\text{re}}} \right)^{2n_{\text{B}} - |n_w|}, & k > k_{\text{re}}. \end{cases} \quad (59)$$

Here,  $k_{\nu}$  denotes the wavenumber that re-enters the horizon at the time when neutrinos decouple from the thermal bath. The wavenumber  $k_{\text{ssb}}$  corresponds to the scale at which production during the radiation-dominated era surpasses that during the reheating phase. It can be approximately defined as  $k_{\text{ssb}} = \mathcal{A}_1^{1/2} k_{\nu} / \ln(k_{\text{re}}/k_{\nu}) \simeq 10^{-1} k_{\nu}$ . Conversely, for couplings with  $n < -1/2$ , the electric field is dominant, and after reheating, only a weak residual magnetic field remains. Consequently, contributions from the magnetic field are negligible in comparison to the primary electric field contributions. The SGW spectrum in this case primarily follows

$$\Omega_{\text{gw,pinf}}^{\text{sec}}(k)h^2 \simeq 2.26 \times 10^{-26} \left( \frac{\Omega_R h^2}{4.3 \times 10^{-5}} \right) \left( \frac{H_{\text{I}}}{10^{-5} M_{\text{P}}} \right)^4 \left( \frac{k_{\text{re}}}{k_{\text{e}}} \right)^{2(n_w + n_{\text{E}})} \mathcal{C}_{\beta}^2(n_{\text{E}}) \mathcal{F}_{n_{\text{E}}}(k) \times \begin{cases} \mathcal{A}_1 \left( \frac{k}{k_{\text{re}}} \right)^{2n_{\text{E}}}, & k_* < k < k_{\text{re}}, \\ \mathcal{A}_2 \left( \frac{k}{k_{\text{re}}} \right)^{2n_{\text{E}} - |n_w|}, & k > k_{\text{re}}. \end{cases} \quad (60)$$

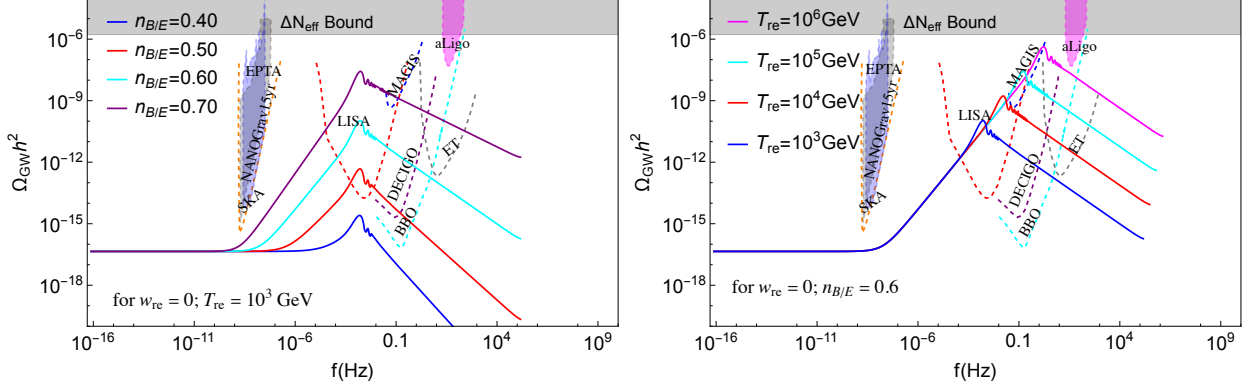


FIG. 2: In this figure, we plot  $\Omega_{\text{gw}} h^2$  versus  $f$  (in Hz) for  $w_{\text{re}} = 0$  for both scenarios,  $n > 1/2$  and  $n < -1/2$ . In the left panel, we consider different values of the magnetic or electric spectral index while keeping the reheating temperature fixed at  $T_{\text{re}} = 10^3$  GeV. In the right panel, we show the dependence of the GW spectra on the reheating temperature for a fixed value of the magnetic (or electric) spectral index.

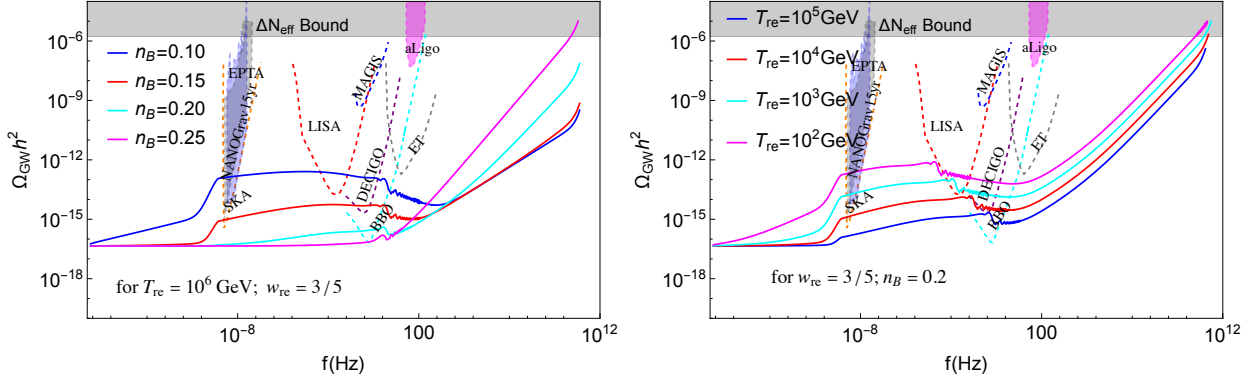


FIG. 3: In the above figure, we plot  $\Omega_{\text{gw}} h^2$  as a function of frequency  $f$  (in Hz) for magnetogenesis scenarios with  $n > 1/2$ , where the magnetic field strength is greater than that of the electric field. In the left panel, we show how the spectrum depends on the magnetic spectral index for a fixed reheating scenario with  $w_{\text{re}} = 3/5$  and  $T_{\text{re}} = 10^6$  GeV. In the right panel, we illustrate the dependence of the reheating temperature on the GW spectrum for a fixed value of  $n_B = 0.2$  and  $w_{\text{re}} = 3/5$ .

For  $n > 1/2$ , the overall spectrum includes additional spectral breaks, as magnetic fields contribute to GW production up to the neutrino decoupling era. In contrast, for  $n < -1/2$ , the high-conductivity post-reheating environment washes out the electric field, leaving only a small magnetic field contribution, making the SGW signal significantly weaker than primary contributions. Note that the quantities  $\mathcal{A}_1$  and  $\mathcal{A}_2$  are listed in Appendix A.

**b. Infinite Electrical Conductivity During the Reheating Era:** In scenarios with infinite electrical conductivity during reheating, the electric fields vanish, implying that any contributions from electric fields originate solely from inflationary production. For the case  $n < -1/2$ , where electric fields dominate, the spectrum follows Eq. (58) for both  $w_{\text{re}} < 1/3$  and  $w_{\text{re}} > 1/3$  reheating scenarios.

Conversely, for  $n > 1/2$ , magnetic fields dominate, and the resulting spectrum follows the form given in Eq. (58) for  $w_{\text{re}} < 1/3$ , or Eq. (59) for  $w_{\text{re}} > 1/3$ .

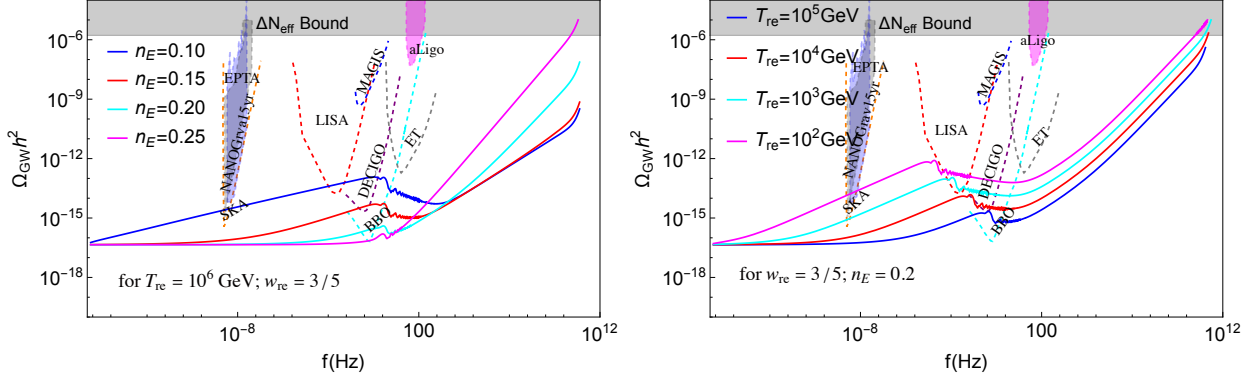


FIG. 4: In the figures above, we have plotted  $\Omega_{\text{gw}} h^2$  as a function of frequency  $f$  (in Hz) for the coupling  $n < -1/2$ , assuming zero electrical conductivity during the reheating era. In the left panel, we show the dependence of the coupling parameter  $n$  ( $n_E$ ) for a fixed reheating scenario with  $w_{\text{re}} = 3/5$  and  $T_{\text{re}} = 10^6$  GeV. In the right panel, we display the dependence of the reheating temperature on the GW spectrum for a fixed equation of state  $w_{\text{re}} = 3/5$  and a fixed magnetogenesis coupling parameter  $n = 1.9$  ( $n_E = 0.2$ ).

#### IV. RESULTS AND DISCUSSION:

In Fig. (2), we plot  $\Omega_{\text{gw}} h^2$  as a function of present-day observable frequency  $f$  (Hz) for a reheating scenario with  $w_{\text{re}} = 0$ , where the universe behaves as a matter-like fluid. The left panel illustrates the dependency on the initial electromagnetic profile for couplings  $n > 1/2$  and  $n < -1/2$ , while the right panel shows dependency on the duration of reheating. For  $n > 1/2$ , where magnetic fields dominate during inflation, the entire SGW spectrum originates from these fields. In contrast, for  $n < -1/2$ , the electric field dominates, making the GW spectral index dependent on the electric spectral index  $n_E$ . Both fields show similar spectral behavior under a sign change in  $n$ , resulting in similar GW spectra when  $w_{\text{re}} < 1/3$ , where inflationary GW production dominates. On large scales, the spectrum is scale-invariant, while sub-horizon modes re-entering before reheating end show a red-tilted spectrum for  $f > f_{\text{re}}$ , scaling as  $f^{2n_B - |n_w|}$  for  $w_{\text{re}} < 1/3$ . In the plot we consider  $w_{\text{re}} = 0$  for which  $n_w = 2(1 - 3w_{\text{re}})/(1 + 3w_{\text{re}}) = 2$ . Increasing the reheating temperature effectively shortens the duration of the reheating phase, thereby shifting the peak frequency of the gravitational wave spectrum toward higher values. In both figures, the large-wavelength (low-frequency) modes exhibit a scale-invariant gravitational wave spectrum, i.e.,  $\Omega_{\text{gw}} h^2(f \ll f_{\text{re}}) \propto f^0$ . This behavior arises from the contribution of primordial gravitational waves (PGWs). Since we consider blue-tilted electromagnetic (EM) fields, most of the magnetic energy is stored in high-frequency modes. At low frequencies, however, the dominant contribution comes from PGWs, which are generated from vacuum fluctuations during inflation and possess a scale-invariant spectrum (see Eq. (57)).

In Fig.(3), we plot  $\Omega_{\text{gw}} h^2$  for  $w_{\text{re}} > 1/3$ , with coupling  $n > 1/2$  where the magnetic field is dominant. Larger values of  $n_B$  yield spectra that can exceed upper bounds set by  $\Delta N_{\text{eff}}$  constraints[83]. Lower values of  $n_B$ , however, are consistent with  $\Delta N_{\text{eff}}$  and tensor-to-scalar ratio bounds and introduce additional spectral breaks. In the range  $f_{\nu} < f < f_{\text{re}}$ , SGWs from the radiation-dominated era exceed those produced during reheating. At high frequencies,  $f \gg f_{\text{re}}$ , the spectrum follows  $f^{2n_B + |n_w|}$  as inflationary SGW production dominates. The left panel shows the dependence on the magnetic spectral index for  $w_{\text{re}} = 3/5$  with  $T_{\text{re}} = 10^6$  GeV, while the right panel examines reheating duration dependency for fixed  $w_{\text{re}} = 3/5$  and  $n_B = 0.2$ . As reheating temperature decreases, the GW amplitude is enhanced by  $(k_{\text{re}}/k_e)^{|n_w|}$ , as the background energy density dilutes faster than the GW density. At very high frequencies, i.e.,  $f \gg f_{\text{re}}$ , the gravitational wave spectrum follows a simple scaling,  $\Omega_{\text{gw}} h^2 \propto f^{0.57}$ , for all parameter sets, differing only in amplitude. This behavior arises from the contribution of primordial gravitational waves (PGWs) at these scales. As is well known, for  $w_{\text{re}} > 1/3$ , the PGW spectrum is blue-tilted, scaling as  $\Omega_{\text{gw}}^{\text{pri}}(f) \propto f^{-n_w}$  (see Eq. (57)). Since we have fixed  $w_{\text{re}} = 3/5$ , the spectral index at very high frequencies is determined by  $n_w$ . The overall amplitude, however, varies depending on the reheating temperature. A lower reheating temperature implies that sub-horizon modes spend a longer time during the reheating phase, leading to greater enhancement of their amplitudes compared to scenarios with higher reheating temperatures.

In Fig. 4, we present the gravitational wave (GW) spectrum  $\Omega_{\text{gw}} h^2$  for  $n < -1/2$ , where electric fields dominate during inflation. Assuming zero electrical conductivity during reheating, electric fields remain unsup-

$w_{re}$	$n_B = 0.01$	$n_B = 0.1$	$n_B = 0.2$	$n_B = 0.3$	$n_B = 0.4$
	$T_{re} \text{ (GeV)}$	$T_{re} \text{ (GeV)}$	$T_{re} \text{ (GeV)}$	$T_{re} \text{ (GeV)}$	$T_{re} \text{ (GeV)}$
0.4	$1.77 \times 10^9$	—	—	—	—
0.5	$5.65 \times 10^{12}$	$1.28 \times 10^7$	2.89	—	—
0.6	$8.2 \times 10^{13}$	$1.46 \times 10^{10}$	$5.41 \times 10^5$	—	—
0.7	$3.59 \times 10^{14}$	$4.86 \times 10^{11}$	$1.92 \times 10^8$	$4.82 \times 10^4$	7.91

TABLE II: In the table above, we’ve listed the minimum reheating temperature for various equations of states (denoted as  $w_{re}$ ), considering five different values of the magnetic spectral index (denoted as  $n_B$ ).

pressed and significantly contribute to GW production in the intermediate frequency range. In this scenario, there are two distinct phases during which electric fields can source gravitational waves: (i) the inflationary epoch and (ii) the reheating era, enabled by the assumption of vanishing conductivity. After reheating ends, the universe enters the standard radiation-dominated phase, during which the plasma conductivity becomes large. Consequently, electric fields—especially those on sub-horizon scales—are rapidly dissipated due to the prompt response of the charged particles, and thus contribute negligibly to the GW background in this era, even when considering reheating scenarios with  $w_{re} > 1/3$ . The shape of the spectrum in this case is characteristically distinct. At high frequencies, the dominant contribution arises from primordial gravitational waves (PGWs), and the spectrum follows  $\Omega_{gw} h^2 \propto f^{-n_w}$ . At low frequencies ( $f < f_{re}$ ), the spectrum exhibits a blue tilt,  $\Omega_{gw} h^2 \propto f^{2n_E}$ , which is only possible if secondary gravitational waves (SGWs), sourced by the electric fields, dominate over the PGWs. This condition depends sensitively on the inflationary coupling parameter  $n$ , as well as the reheating parameters  $w_{re}$  and  $T_{re}$ . Furthermore, for certain parameter choices, we observe that the GW spectrum remains scale-invariant at CMB scales, indicating PGW dominance at those wavelengths. Additionally, decreasing the reheating temperature for fixed  $w_{re}$  and  $n_E$  (see the right panel of Fig. 4) leads to an overall enhancement in GW amplitude, due to the prolonged duration of reheating. This also shifts the spectral break near  $f \sim f_{re}$  toward lower frequencies.

**a. Constraining model parameters through the Tensor-to-Scalar Ratio  $r$ :** This magnetogenesis model generates significant electric and magnetic fields capable of producing gravitational waves (GWs) strong enough to pass various sensitivity thresholds and create notable tensor fluctuations at CMB scales. For  $w_{re} > 1/3$  reheating scenarios, the reheating dynamics introduce an overall enhancement factor,  $(k_e/k_{re})^{|n_w|}$ , related to the duration of the reheating phase. However, constraints on tensor fluctuations at CMB scales, quantified by the tensor-to-scalar ratio  $r_{0.05}$ , place a limit on GW strength at the pivot scale:  $\Omega_{gw} h^2 \leq 1.14 \times 10^{-7} r_{0.05} A_s$ . Here,  $A_s \simeq 2.1 \times 10^{-9}$  is the current bound on the scalar amplitude at the pivot scale.

Using the limit  $r_{0.05} \leq 0.036$ , we find that the coupling parameter  $n$  for magnetogenesis should satisfy  $-2.1 \leq n \leq 2.1$ . This bound holds universally, even for instantaneous reheating. For prolonged reheating scenarios with  $w_{re} > 1/3$ , these constraints become more robust, limiting both the reheating dynamics and the magnetogenesis model. Thus, utilizing the upper bound  $r_{0.05} \leq 0.036$  at the pivot scale, we derive the following constraint,

$$1 \geq \frac{182 r A_s \mathcal{A}_1}{(3 - 2n_B)} \left( \frac{k_e}{k_{re}} \right)^{2|n_w|} \left( \frac{k_*}{k_e} \right)^{2n_B} \mathcal{C}_{B/E}^2(n_{B/E}). \quad (61)$$

Using this constraint, we set bounds on the reheating temperature for specific values of the equation of state (EoS) across five discrete values of the magnetic spectral index  $n_{B/E} = 0.01, 0.1, 0.2, 0.3$ , and  $0.4$ , as shown in Table (II). In our analysis, we treat the reheating equation-of-state parameter  $w_{re}$  as a free parameter, allowing it to take arbitrary values. However, in specific inflationary models—for example, those with power-law potentials of the form  $V(\phi) \propto \phi^{2n}$ ,  $w_{re}$  can be uniquely determined based on the dynamics of the scalar field. In this work, we adopt a generalized approach by leaving  $w_{re}$  unconstrained. As an illustration, to avoid the overproduction of tensor perturbations at CMB scales, consider the case where the magnetic spectral index is  $n_B = 0.01$  (nearly scale-invariant). For a reheating equation-of-state  $w_{re} = 0.4$ , the lower bound on the reheating temperature is found to be  $T_{re}^{\min} \simeq 1.77 \times 10^9 \text{ GeV}$ . If the reheating temperature falls below this value, electromagnetic fields generated via this mechanism can produce excessive tensor fluctuations at large scales, violating current observational constraints on the tensor-to-scalar ratio. We summarize the lower bounds on reheating temperatures for various parameter combinations in Table (II).

**b. Constraining Reheating and Magnetogenesis Parameters through  $\Delta N_{\text{eff}}$  Bound:** During the epoch of decoupling, the CMB is influenced by the total radiation energy density. Any excess energy that

behaves as radiation-like fields may impact the CMB [84]. In our case, the primordial GWs carry significant energy, and since GWs evolve as  $a^{-4}$  like radiation, frequencies  $f > 10^{-15}$  Hz can be treated as extra radiation energy that may affect the CMB (see related discussions in [85, 86]). This excess radiation can be quantified by the additional relativistic degrees of freedom at decoupling, expressed as  $\Delta N_{\text{eff}}$ , indicating the extra neutrino species predicted beyond the Standard Model. Using this, we derive the following constraint [28, 85],

$$\Delta N_{\text{eff}} \geq \frac{1}{\Omega_\gamma h^2} \frac{8}{7} \left( \frac{11}{4} \right)^{4/3} \int_{k_0}^{k_f} \frac{dk}{k} \Omega_{\text{gw}} h^2(k). \quad (62)$$

Assuming the present-day photon density parameter as  $\Omega_\gamma h^2 \simeq 2.48 \times 10^{-5}$ , the combined latest Planck-2018 and Baryon Acoustic Oscillation (BAO) data predict  $\Delta N_{\text{eff}} \simeq 0.284$  (within a  $2\sigma$  range) [87], setting an upper bound on primordial GWs,  $\Omega_{\text{gw}} h^2 < 1.67 \times 10^{-6}$  [83].

At high frequencies, the GW spectrum behaves as  $\Omega_{\text{gw}} h^2 \propto f^{2n_B}$  for  $f < f_{\text{re}}$ , while for modes well within the horizon ( $f \gg f_{\text{re}}$ ), it follows  $\Omega_{\text{gw}} h^2 \propto f^{2n_B - n_w}$ . Therefore, if  $2n_B > n_w$ , the spectrum has a red tilt for  $f > f_{\text{re}}$ ; otherwise, it has a blue tilt. Using this bound, we find that for reheating scenarios with  $w_{\text{re}} = 0$ , the maximum allowed magnetic spectral index consistent with the  $\Delta N_{\text{eff}}$  bound is  $n_B \leq 1.0$ . This constraint also restricts the reheating temperature for a fixed magnetic spectral index and equation of state (EoS). For instance, with  $w_{\text{re}} = 0$  and  $n_B = 1.0$ , the reheating temperature should be below  $T_{\text{re}} < 10^3$  GeV. For  $n_B = 0.9$  and  $w_{\text{re}} = 0$ , a more relaxed bound is obtained:  $T_{\text{re}} \leq 10^7$  GeV.

For higher EoS,  $w_{\text{re}} > 1/3$ , at high frequencies with  $n_B > 0.3$ , the GW spectrum follows  $\Omega_{\text{gw}} h^2 \propto f^{2n_B + |n_w|}$ . In this regime, secondary GW production during inflation is more substantial compared to late-time production, and since the background dilutes faster than the GW energy density (for  $w_{\text{re}} > 1/3$  scenarios), these frequency modes are more enhanced. Thus, for  $w_{\text{re}} > 1/3$ , this bound imposes even stronger constraints on both the magnetic spectral index and reheating dynamics.

**c. Non-helical magnetogenesis in light of PTA:** The Stochastic Gravitational-Wave Background (SGWB) is a prominent prediction from numerous astrophysical and cosmological phenomena, especially within Early Universe Cosmology. Recent advancements in pulsar timing arrays (PTAs) have led to significant breakthroughs, resulting in the detection of the SGWB [6, 8, 10, 88]. Additionally, a thorough analysis of the Hellings-Downs (HD) correlation of timing residuals has provided substantial evidence for the SGWB, clarifying the observed power-law excess. Notably, the significance of the HD correlation for various PTAs falls approximately within  $3\sigma$  for NANOGrav [6],  $3\sigma$  for EPTA [88],  $2\sigma$  for PPTA, and an impressive  $4.5\sigma$  [8] for CPTA [10] observations, respectively.

As observed, inflationary magnetogenesis models can produce sufficient GW strength to surpass vacuum production in intermediate frequency ranges. For  $n_B > 0$ , with appropriate reheating parameters, we can generate blue-tilted GW at intermediate frequencies. From the  $\Delta N_{\text{eff}}$  bound, we found that for  $w_{\text{re}} > 1/3$  reheating scenarios, the magnetic spectral index  $n_B$  (or electric spectral index  $n_E$ ) must be tightly constrained to avoid excessive GW production at very high frequencies, where the GW spectrum scales as  $\Omega_{\text{gw}} h^2 \propto f^{2n_B + |n_w|}$  for  $w_{\text{re}} > 1/3$ . This is illustrated in Fig. (3). Meanwhile, PTA observations indicate that the spectrum should exhibit a strong blue tilt at nano-Hz frequencies, with a GW spectrum scaling as  $\Omega_{\text{gw}} h^2 \propto f^{0.91}$  for NANOGrav 15 yr data [6]. Here we have found that for  $w_{\text{re}} < 1/3$  reheating scenarios, the GW spectrum produced from the EM field behaves as  $\Omega_{\text{gw}} h^2 \propto f^{2n_{B/E} - |n_w|}$ , so to get a strongly blue tilted GW spectrum at the nano-Hz frequency range, the lower EoS ( $w_{\text{re}} < 1/3$ ) is more favored compared to  $w_{\text{re}} > 1/3$  scenarios.

For this analysis, we employed the PTARcade code [89] for MCMC analysis to determine the best-fit parameter values, restricting our scenarios to  $w_{\text{re}} < 1/3$  reheating cases and running the PTARcade code. We selected the following priors:  $w_{\text{re}} \sim \mathcal{U}(0, 1/3)$ ,  $n_B \sim \mathcal{U}(0, 1.2)$ , and  $\log_{10}(T_{\text{re}}) \sim \mathcal{U}(-2, 1)$ . The predicted parameters and their  $1\sigma$  tolerance range, along with the corresponding Bayesian factor, are listed in Tab. (IV 0c). The posterior distributions of the predicted parameters are shown in Fig. (5) for two different runs ( $R1, R2$ ) corresponding to two different priors of  $n_B \in (0, 1.0)$  and  $n_B \in ((0, 1.5))$  respectively. Our analysis indicates that, to match current data, this model can only produce a GW signal consistent with both amplitude and slope if  $n_B \simeq 1.21_{-0.12}^{+0.1}$ . Note the  $n_B$  is greater than unity. Let us remind that for  $w_{\text{re}} < 1/3$ , the GW spectrum exhibits a blue tilt for  $f > f_{\text{re}}$ , with  $\Omega_{\text{gw}} h^2 \propto f^{2n_B - |n_w|}$ . Where  $n_w = 2(1 - 3n_w)/(1 + 3n_w) \leq 2$ . Hence, for  $n_B > 1.0$ , the GW spectrum exhibits a blue tilt at high frequency for  $f > f_{\text{re}}$ . Consequently, it again violates  $\Delta N_{\text{eff}}$  bound. Including other PTA observations, such as those from the European PTA (EPTA) (including data from the Indian PTA (InPTA)) [88], PPTA [8], or CPTA [10], may suggest a slightly lower spectral index. However, we find it difficult, or one needs extreme fine-tuning of the model parameters, to be able to fit the nano-Hz observation.



Model	Parameter	Prior	Posterior	Bayes Factors ( $\mathcal{B}_{X,Y}$ )
<b>R1</b>	$w_{re}$	(0, 0.333)	$0.12^{+0.11}_{-0.08}$	$1.57 \pm 0.19$
	$\log_{10}(T_{re})$	(-2, 1)	$-0.40^{+0.93}_{-1.0}$	
	$n_B$	(0, 1.5)	$0.32^{+0.65}_{-0.10}$	
<b>R2</b>	$w_{re}$	(0, 0.333)	$0.13^{+0.11}_{-0.09}$	$22.77 \pm 7.022$
	$\log_{10}(T_{re})$	(-3, 1)	$-0.38^{+1.06}_{-0.17}$	
	$n_B$	(0, 1.5)	$1.17^{+0.01}_{-0.01}$	

TABLE III: In the table above, we list the posterior distributions of the parameters for our model, obtained from two different runs, *R1* and *R2*. In *R1*, we consider the prior for the magnetic spectral index  $n_B \in (0, 1.0)$ , which is consistent with the  $\Delta N_{\text{eff}}$  bound. In *R2*, we extend the prior range of  $n_B$  to  $(0, 1.5)$ , while keeping the same prior for the other two parameters in both cases. We also include the corresponding Bayes Factor for each run in the table.

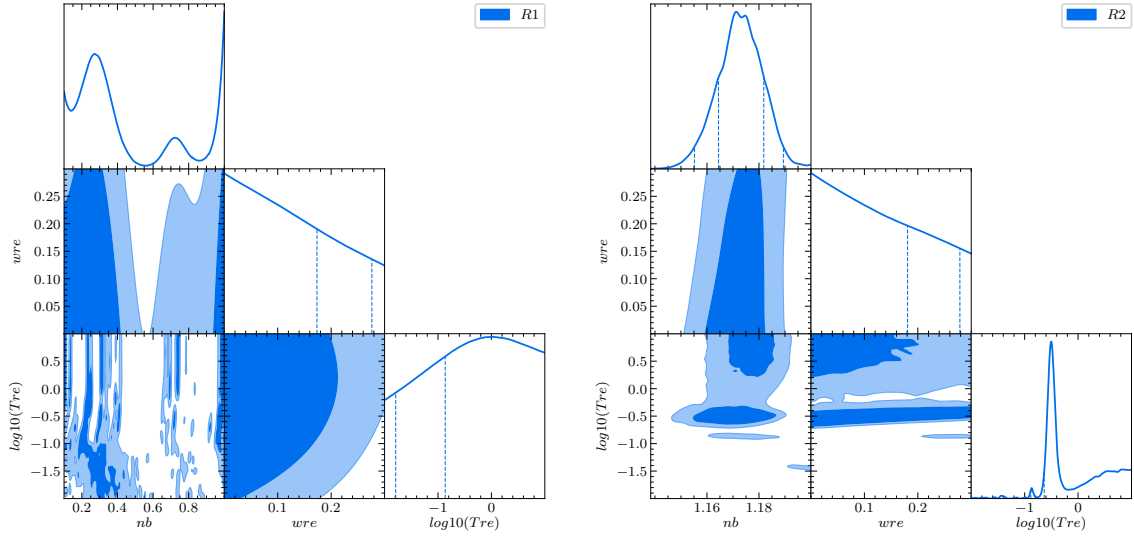


FIG. 5: In the figures presented above, we display the posterior distributions of the parameters governing the Stochastic Gravitational Waves (SGWs) induced by non-helical magnetic fields, generated using the PTARCADE code [89]. The diagonal elements of the corner plot show the 1D marginalized distributions for the parameters  $n_B$ ,  $w_{re}$ , and  $T_{re}$ . In the left figure, we consider a prior for the magnetic spectral index  $n_B \in (0, 1.0)$ , while in the right figure, we consider an extended prior range for  $n_B \in (0, 1.5)$ .

## V. CONCLUSIONS

In this study, we explore the mechanism of magnetic field generation through an  $f^2(\phi)F_{\mu\nu}F^{\mu\nu}$  coupling during inflation and analyze the effects of non-instantaneous reheating scenarios. Specifically, we examine how the electrical conductivity during the reheating phase impacts magnetic field evolution, focusing on two limiting cases: zero and infinite conductivity. Our analysis reveals that non-instantaneous reheating plays a pivotal role in determining the present-day strength of large-scale magnetic fields.

By varying the reheating parameters—namely the effective equation of state  $w_{re}$  and the reheating temperature  $T_{re}$ —we demonstrate that it is possible to satisfy current observational bounds on magnetic fields at Mpc scales, even for blue-tilted spectra with  $n < -1/2$ . For such couplings, we find that the maximum achievable present-day magnetic field strength at the 1 Mpc scale is  $B_0 \sim 2.6 \times 10^{-18}$  G, assuming a radiation-like reheating phase ( $w_{re} = 1/3$ ) with the lowest allowed reheating temperature  $T_{re} \simeq 0.01$  GeV.

In contrast, for a matter-like reheating phase ( $w_{re} = 0$ ) with the same reheating temperature, the maximum attainable field strength drops significantly to  $B_0 \simeq 3.7 \times 10^{-30}$  G. Although this scenario features the longest reheating duration, leading to a higher conversion efficiency of electric to magnetic energy, the enhanced dilution due to background expansion outweighs this benefit, resulting in a much weaker present-day field.



Furthermore, for stiffer equations of state ( $w_{re} > 1/3$ ), the maximum magnetic field strength achievable for  $n < -1/2$  couplings is around  $B_0 \simeq 10^{-23}$  G, while remaining consistent with current constraints on the tensor-to-scalar ratio at CMB scales.

On the other hand, couplings with  $n = 2$  can lead to stronger magnetic fields that exceed the current lower bounds for appropriate reheating parameters. However, such models suffer from the well-known strong coupling problem, which limits their viability despite their potential for generating larger magnetic fields.

In the second part of this work, we explored the potential detectability of our magnetogenesis scenario under generalized reheating dynamics, where both the effective equation of state parameter  $w_{re}$  and the reheating temperature  $T_{re}$  are treated as free parameters. We find that non-instantaneous reheating has a significant impact on the resulting gravitational wave (GW) spectrum.

Specifically, for matter-like reheating ( $w_{re} = 0$ ), the combined gravitational wave (GW) spectrum—comprising both primordial GWs (PGWs) and sourced GWs (SGWs)—exhibits two distinct spectral breaks. In contrast, stiff-like reheating scenarios with  $w_{re} > 1/3$  produce multiple spectral breaks, which provide a clear signature for distinguishing them from other cases. Remarkably, for  $w_{re} > 1/3$  and coupling indices  $n > 1/2$ , the GW spectrum can feature up to five spectral breaks. On the other hand, for models with  $n < -1/2$ , where electric fields dominate and electrical conductivity is negligible, the spectrum shows a maximum of three spectral breaks. These distinctive features not only serve as unique identifiers for inflationary magnetogenesis models but also offer crucial information about early-universe microphysics, such as the conductivity behavior during reheating.

We also show that in these non-trivial reheating scenarios with  $w_{re} \neq 1/3$ , the tensor perturbations sourced by magnetic fields at CMB scales are modified by reheating dynamics. This opens the possibility of constraining reheating through CMB observations of the tensor-to-scalar ratio or, conversely, constraining the magnetogenesis model for a given reheating scenario.

Finally, we investigated whether such magnetogenesis models can be constrained by current Pulsar Timing Array (PTA) observations. While non-helical models cannot explain the current PTA signals due to limits from  $\Delta N_{eff}$ , our analysis shows that if the conductivity during reheating is indeed small, possibly due to the absence or transition of charged particles, the resulting GW signals could pass through the sensitivity curves of upcoming detectors such as LISA, BBO, and DECIGO. These signals also exhibit unique spectral features that are sensitive not only to the initial magnetic field spectrum but also to the details of post-inflationary evolution. Our findings suggest that future GW observations could simultaneously probe inflation, reheating, and magnetogenesis, offering a new window into the early universe.

### Acknowledgments

SM gratefully acknowledges financial support from the Council of Scientific and Industrial Research (CSIR), Ministry of Science and Technology, Government of India. SM also thanks Prof. L. Sriramkumar for insightful and fruitful discussions related to this work. DM wishes to acknowledge support from the Science and Engineering Research Board (SERB), Department of Science and Technology (DST), Government of India (GoI), through the Core Research Grant CRG/2020/003664. We want to thank our Gravity and High Energy Physics groups at IIT Guwahati for illuminating discussions.

### Appendix A: Calculation of the coefficient $\mathcal{A}_1$ , $\mathcal{A}_2$ & $\mathcal{A}_3$ :

The tensor power spectrum sourced by electromagnetic fields at the end of reheating is given by

$$\mathcal{P}_{T,s}^{re} = \frac{2H_1^4}{M_P^4} \left( \frac{k}{k_e} \right)^{2(\delta-2)} \mathcal{C}_{B/E}^2(n_{B/E}) \left( \frac{k}{k_e} \right)^{2n_{B/E}} \mathcal{C}_{m,re}^2(x_{re}, x_{end}) \mathcal{F}_{n_{B/E}}(k), \quad (\text{A1})$$

where the time-dependent integral part  $\mathcal{C}_{m,re}(x_{re}, x_{end})$  is defined as [28]

$$\mathcal{C}_{m,re}(x_{re}, x_{end}) = \int_{x_{end}}^{x_{re}} dx_1 x_1^{-\delta} \mathcal{G}_{\mathbf{k}}(x_{re}, x_1), \quad (\text{A2})$$

with  $\mathcal{G}_{\mathbf{k}}(x, x_1)$  being the Green's function associated with tensor perturbations. During the reheating era, this Green's function takes the form [28]

$$\mathcal{G}_{\mathbf{k}}(x, x_1) = \theta(x - x_1) \frac{\pi x^l x_1^{1-l}}{2k \sin(l\pi)} [J_l(x) J_{-l}(x_1) - J_{-l}(x) J_l(x_1)] \quad (\text{A3})$$

Substituting Eq.(A3) into Eq.(A2), we obtain

$$\begin{aligned} \mathcal{C}_{\text{m, re}}(x, x_1) &= \frac{\pi x^l}{2 \sin(l\pi)} \int dx_1 x_1^{1-l-\delta} [J_l(x) J_{-l}(x_1) - J_{-l}(x) J_l(x_1)] \\ &= 2^{-2-l} x^l x_1^{2-2l-\delta} \left\{ \frac{\Gamma(-l) \Gamma[1 - (\delta/2)]}{\Gamma[2 - (\delta/2)]} x_1^{2l} J_{-l}(x) {}_1F_2[1 - (\delta/2); 1 + l, 2 - (\delta/2); -(x_1^2/4)] \right. \\ &\quad \left. + 4^l \frac{\Gamma(l) \Gamma[1 - l - (\delta/2)]}{\Gamma[2 - l - (\delta/2)]} J_l(x) {}_1F_2[1 - l - (\delta/2); 1 - l, 2 - l - (\delta/2); -(x_1^2/4)] \right\}, \end{aligned} \quad (\text{A4})$$

where  ${}_1F_2(a, b, c, z)$  denotes the hypergeometric function.

*a. Spectral shape of  $\Omega_{\text{GW}}$  for  $k < k_{\text{re}}$  and  $k \gg k_{\text{re}}$*

For wave numbers satisfying  $k \ll k_{\text{re}}$ , we consider the regime where  $x_{\text{end}} \ll x_{\text{re}} \ll 1$ . In this limit, the integral  $\mathcal{C}_{\text{m, re}}(x_{\text{re}}, x_{\text{end}})$  simplifies significantly and can be approximated as

$$\lim_{k \ll k_{\text{re}}} \mathcal{C}_{\text{m, re}}(x_{\text{re}}, x_{\text{end}}) \simeq \frac{1}{(1 - \delta)^2} \left\{ \frac{2}{1 + 2\delta} - \frac{2}{2 - \delta} \left[ 1 - \left( \frac{k_{\text{re}}}{k_e} \right)^{2-\delta} \right] \right\} \left( \frac{k}{k_{\text{re}}} \right)^{2-\delta}. \quad (\text{A5})$$

Similarly, when  $k \gg k_{\text{re}}$ , for  $w_{\text{re}} > 1/3$ , the quantity  $\mathcal{C}_{\text{m, re}}(x_{\text{re}}, x_{\text{end}})$  reduces to

$$\begin{aligned} \lim_{k \gg k_{\text{re}}} \mathcal{C}_{\text{m, re}}(x_{\text{re}}, x_{\text{end}}) &\simeq \sqrt{\frac{2}{\pi}} \frac{2^{(1-\delta)/2}}{(1 - \delta)} \Gamma[(3 - \delta)/2] \Gamma[(\delta - 1)/2] x_{\text{re}}^{-\delta/2} \left\{ \frac{\Gamma[(1 - \delta)/2]}{\Gamma(\delta/2)} \cos[x_{\text{re}} - (2 - \delta)\pi/4] \right. \\ &\quad \left. - \frac{2}{2 - \delta} \cos[x_{\text{re}} - \delta\pi/4] \right\}, \end{aligned} \quad (\text{A6})$$

whereas, for  $w_{\text{re}} < 1/3$ , the quantity simplifies to

$$\begin{aligned} \lim_{k \gg k_{\text{re}}} \mathcal{C}_{\text{m, re}}(x_{\text{end}}, x_{\text{re}}) &\simeq \sqrt{\frac{2}{\pi}} \frac{2^{(\delta-3)/2}}{(1 - \delta)} \frac{\Gamma[(\delta - 1)/2] \Gamma[1 - (\delta/2)]}{\Gamma[2 - (\delta/2)]} x_{\text{re}}^{-\delta/2} x_{\text{end}}^{2-\delta} \cos[-x_{\text{re}} + \delta\pi/4] \\ &\simeq \sqrt{\frac{2}{\pi}} \frac{2^{(\delta-3)/2} \Gamma[\frac{\delta-1}{2}]}{(1 - \delta)(1 - \delta/2)} x_{\text{re}}^{-\delta/2} x_{\text{end}}^{2-\delta} \cos[x_{\text{re}} - (2 - \delta)\pi/4]. \end{aligned} \quad (\text{A7})$$

At the end of reheating, the power spectrum of secondary GWs generated due to the magnetic fields [defined in Eq. (51)] is given by

$$\mathcal{P}_{T,s}^{\text{re}} = \frac{2H_{\text{I}}^4}{M_{\text{P}}^4} \left( \frac{k}{k_e} \right)^{2(\delta-2)} \mathcal{C}_{\text{B/E}}^2(n_{\text{B/E}}) \left( \frac{k}{k_e} \right)^{2n_{\text{B/E}}} \mathcal{C}_{\text{m, re}}^2(x_{\text{re}}, x_{\text{end}}) \mathcal{F}_{n_{\text{B/E}}}(k), \quad (\text{A8})$$

On substituting Eq. (A5) in this expression, for  $k \ll k_{\text{re}}$ , we obtain that

$$\lim_{k \ll k_{\text{re}}} \mathcal{P}_{T,s}^{\text{re}}(k, \eta_{\text{re}}) \simeq \mathcal{A}_1 \left( \frac{H_{\text{I}}}{M_{\text{P}}} \right)^4 \left( \frac{k_{\text{re}}}{k_e} \right)^{2(\delta-2)} \left( \frac{k}{k_e} \right)^{2n_{\text{B/E}}} \mathcal{C}_{\text{B/E}}^2(n_{\text{B/E}}) \mathcal{F}_{n_{\text{B/E}}}(k) \quad (\text{A9})$$

Similarly, on utilizing Eqs. (A6) and (A7), for  $k > k_{\text{re}}$ , we obtain the following expressions

$$\lim_{k > k_{\text{re}}} \mathcal{P}_{T,s}^{\text{re}}(k, \eta_{\text{re}}) \simeq \mathcal{A}_2 \left( \frac{H_{\text{I}}}{M_{\text{P}}} \right)^4 \left( \frac{k_{\text{re}}}{k_e} \right)^{2(\delta-2)} \left( \frac{k}{k_{\text{re}}} \right)^{-2-|n_w|} \left( \frac{k}{k_e} \right)^{2n_{\text{B}}} \mathcal{C}_{\text{B/E}}^2(n_{\text{B/E}}) \mathcal{F}_{n_{\text{B/E}}}(k); \text{ for } w_{\text{re}} > 1/3 \quad (\text{A10a})$$

$$\lim_{k > k_{\text{re}}} \mathcal{P}_{T,s}^{\text{re}}(k, \eta_{\text{re}}) \simeq \mathcal{A}_3 \left( \frac{H_{\text{I}}}{M_{\text{P}}} \right)^4 \left( \frac{k_{\text{re}}}{k_e} \right)^{2(\delta-2)} \left( \frac{k}{k_{\text{re}}} \right)^{-2-|n_w|} \left( \frac{k}{k_e} \right)^{2n_{\text{B}}} \mathcal{C}_{\text{B/E}}^2(n_{\text{B/E}}) \mathcal{F}_{n_{\text{B/E}}}(k); \text{ for } w_{\text{re}} < 1/3, \quad (\text{A10b})$$

where we defined the quantities  $\mathcal{A}_1$ ,  $\mathcal{A}_2$  and  $\mathcal{A}_3$  that appear in the above expressions are given by

$$\mathcal{A}_1 = \frac{2}{(1-\delta)^4} \left\{ \frac{2}{1+2\delta} - \frac{2}{2-\delta} \left[ 1 - \left( \frac{k_{\text{re}}}{k_e} \right)^{2-\delta} \right] \right\}^2, \quad (\text{A11a})$$

$$\mathcal{A}_2 = \frac{2^{(3-\delta)} \Gamma^2[(3-\delta)/2] \Gamma^2[(\delta-1)/2]}{\pi(1-\delta)^2} \left\{ \frac{\Gamma[(1-\delta)/2]}{\Gamma(\delta/2)} \cos[(k/k_{\text{re}}) - (2-\delta)\pi/4] - \frac{2}{2-\delta} \cos[(k/k_{\text{re}}) - \delta\pi/4] \right\}^2, \quad (\text{A11b})$$

$$\mathcal{A}_3 = \frac{2^{\delta-1} \Gamma^2[(\delta-1)/2]}{\pi(1-\delta)^2(1-\delta/2)^2} \left( \frac{k_{\text{re}}}{k_e} \right)^{2(2-\delta)} \cos^2[(k/k_{\text{re}}) - \delta\pi/4]. \quad (\text{A11c})$$

- 
- [1] B. P. Abbott *et al.* (LIGO Scientific, Virgo), *Phys. Rev. Lett.* **116**, 061102 (2016), [arXiv:1602.03837 \[gr-qc\]](#).
  - [2] B. P. Abbott *et al.* (LIGO Scientific, Virgo), *Phys. Rev. Lett.* **116**, 241102 (2016), [arXiv:1602.03840 \[gr-qc\]](#).
  - [3] B. P. Abbott *et al.* (LIGO Scientific, Virgo), *Phys. Rev. Lett.* **116**, 131103 (2016), [arXiv:1602.03838 \[gr-qc\]](#).
  - [4] B. P. Abbott *et al.* (LIGO Scientific, Virgo), *Phys. Rev. D* **93**, 122003 (2016), [arXiv:1602.03839 \[gr-qc\]](#).
  - [5] B. P. Abbott *et al.* (LIGO Scientific, VIRGO), *Phys. Rev. Lett.* **118**, 221101 (2017), [Erratum: *Phys. Rev. Lett.* **121**, 129901 (2018)], [arXiv:1706.01812 \[gr-qc\]](#).
  - [6] G. Agazie *et al.* (NANOGrav), *Astrophys. J. Lett.* **951**, L8 (2023), [arXiv:2306.16213 \[astro-ph.HE\]](#).
  - [7] J. Antoniadis *et al.*, (2023), [10.1051/0004-6361/202346841](#), [arXiv:2306.16224 \[astro-ph.HE\]](#).
  - [8] D. J. Reardon *et al.*, *Astrophys. J. Lett.* **951**, L6 (2023), [arXiv:2306.16215 \[astro-ph.HE\]](#).
  - [9] A. Zic *et al.*, (2023), [arXiv:2306.16230 \[astro-ph.HE\]](#).
  - [10] H. Xu *et al.*, *Res. Astron. Astrophys.* **23**, 075024 (2023), [arXiv:2306.16216 \[astro-ph.HE\]](#).
  - [11] A. A. Starobinsky, *JETP Lett.* **30**, 682 (1979).
  - [12] L. P. Grishchuk, *Zh. Eksp. Teor. Fiz.* **67**, 825 (1974).
  - [13] M. C. Guzzetti, N. Bartolo, M. Liguori, and S. Matarrese, *Riv. Nuovo Cim.* **39**, 399 (2016), [arXiv:1605.01615 \[astro-ph.CO\]](#).
  - [14] M. R. Haque, D. Maity, T. Paul, and L. Sriramkumar, *Phys. Rev. D* **104**, 063513 (2021), [arXiv:2105.09242 \[astro-ph.CO\]](#).
  - [15] C. Caprini and R. Durrer, *Phys. Rev. D* **65**, 023517 (2001).
  - [16] L. Sorbo, *JCAP* **06**, 003 (2011), [arXiv:1101.1525 \[astro-ph.CO\]](#).
  - [17] C. Caprini and L. Sorbo, *JCAP* **10**, 056 (2014), [arXiv:1407.2809 \[astro-ph.CO\]](#).
  - [18] A. Ito and J. Soda, *Phys. Lett. B* **771**, 415 (2017), [arXiv:1607.07062 \[hep-th\]](#).
  - [19] R. Sharma, K. Subramanian, and T. R. Seshadri, *Phys. Rev. D* **101**, 103526 (2020), [arXiv:1912.12089 \[astro-ph.CO\]](#).
  - [20] S. Okano and T. Fujita, *JCAP* **03**, 026 (2021), [arXiv:2005.13833 \[astro-ph.CO\]](#).
  - [21] J. Adams, B. Cresswell, and R. Easther, *Phys. Rev. D* **64**, 123514 (2001).
  - [22] H. Di and Y. Gong, *JCAP* **07**, 007 (2018), [arXiv:1707.09578 \[astro-ph.CO\]](#).
  - [23] C. Fu, P. Wu, and H. Yu, *Phys. Rev. D* **101**, 023529 (2020), [arXiv:1912.05927 \[astro-ph.CO\]](#).
  - [24] H. V. Ragavendra, P. Saha, L. Sriramkumar, and J. Silk, *Phys. Rev. D* **103**, 083510 (2021).
  - [25] N. Bhaumik and R. K. Jain, *Phys. Rev. D* **104**, 023531 (2021), [arXiv:2009.10424 \[astro-ph.CO\]](#).
  - [26] M. Solbi and K. Karami, *JCAP* **08**, 056 (2021), [arXiv:2102.05651 \[astro-ph.CO\]](#).
  - [27] D. G. Figueroa, S. Raatikainen, S. Rasanen, and E. Tomberg, *JCAP* **05**, 027 (2022), [arXiv:2111.07437 \[astro-ph.CO\]](#).
  - [28] S. Maiti, D. Maity, and L. Sriramkumar, (2024), [arXiv:2401.01864 \[gr-qc\]](#).
  - [29] A. Kandus, K. E. Kunze, and C. G. Tsagas, *Phys. Rept.* **505**, 1 (2011), [arXiv:1007.3891 \[astro-ph.CO\]](#).
  - [30] M. S. Turner and L. M. Widrow, *Phys. Rev. D* **37**, 2743 (1988).
  - [31] R. Durrer and A. Neronov, *Astron. Astrophys. Rev.* **21**, 62 (2013), [arXiv:1303.7121 \[astro-ph.CO\]](#).
  - [32] R. J. Z. Ferreira, R. K. Jain, and M. S. Sloth, *JCAP* **10**, 004 (2013), [arXiv:1305.7151 \[astro-ph.CO\]](#).
  - [33] K. Subramanian, *Rept. Prog. Phys.* **79**, 076901 (2016), [arXiv:1504.02311 \[astro-ph.CO\]](#).
  - [34] T. Kobayashi, *JCAP* **05**, 040 (2014), [arXiv:1403.5168 \[astro-ph.CO\]](#).
  - [35] M. R. Haque, D. Maity, and S. Pal, *Phys. Rev. D* **103**, 103540 (2021), [arXiv:2012.10859 \[hep-th\]](#).
  - [36] S. Tripathy, D. Chowdhury, R. K. Jain, and L. Sriramkumar, *Phys. Rev. D* **105**, 063519 (2022), [arXiv:2111.01478 \[astro-ph.CO\]](#).
  - [37] Y. Li and L.-Y. Zhang, *Mod. Phys. Lett. A* **37**, 2250069 (2022).
  - [38] P. Adshead, J. T. Giblin, T. R. Scully, and E. I. Sfakianakis, *JCAP* **10**, 039 (2016), [arXiv:1606.08474 \[astro-ph.CO\]](#).
  - [39] L. Campanelli, *Int. J. Mod. Phys. D* **18**, 1395 (2009), [arXiv:0805.0575 \[astro-ph\]](#).

- [40] R. K. Jain, R. Durrer, and L. Hollenstein, *J. Phys. Conf. Ser.* **484**, 012062 (2014), [arXiv:1204.2409 \[astro-ph.CO\]](#) .
- [41] K. Bamba, S. D. Odintsov, T. Paul, and D. Maity, *Phys. Dark Univ.* **36**, 101025 (2022), [arXiv:2107.11524 \[gr-qc\]](#) .
- [42] S. Maiti, D. Maity, and R. Srikanth, (2025), [arXiv:2504.15400 \[astro-ph.CO\]](#) .
- [43] A. Neronov and I. Vovk, *Science* **328**, 73 (2010).
- [44] W. Essey, S. Ando, and A. Kusenko, *Astropart. Phys.* **35**, 135 (2011), [arXiv:1012.5313 \[astro-ph.HE\]](#) .
- [45] S. Saga, H. Tashiro, and S. Yokoyama, *Phys. Rev. D* **98**, 083518 (2018).
- [46] A. Fletcher, *arXiv preprint arXiv:1104.2427* (2011).
- [47] R. Beck, *The Astronomy and Astrophysics Review* **24**, 4 (2016).
- [48] M. Haverkorn, J. C. Brown, B. M. Gaensler, and N. M. McClure-Griffiths, *Astrophys. J.* **680**, 362 (2008), [arXiv:0802.2740 \[astro-ph\]](#) .
- [49] P. Kronberg, Q. Dufton, H. Li, and S. Colgate, *The Astrophysical Journal* **560**, 178 (2001).
- [50] D. Grasso and H. R. Rubinstein, *Phys. Rept.* **348**, 163 (2001), [arXiv:astro-ph/0009061](#) .
- [51] V. A. Acciari *et al.* (MAGIC), *Astron. Astrophys.* **670**, A145 (2023), [arXiv:2210.03321 \[astro-ph.HE\]](#) .
- [52] K. Takahashi, M. Mori, K. Ichiki, and S. Inoue, *The Astrophysical Journal Letters* **744**, L7 (2011).
- [53] T. C. Arlen, V. V. Vassilev, T. Weisgarber, S. P. Wakely, and S. Y. Shafi, *The Astrophysical Journal* **796**, 18 (2014).
- [54] H. J. Hortúa and L. Castañeda, *Phys. Rev. D* **90**, 123520 (2014), [arXiv:1405.1786 \[gr-qc\]](#) .
- [55] D. Paoletti, J. Chluba, F. Finelli, and J. A. Rubiño Martín, (2022), [10.1093/mnras/stac2947](#), [arXiv:2204.06302 \[astro-ph.CO\]](#) .
- [56] A. Zucca, Y. Li, and L. Pogosian, *Phys. Rev. D* **95**, 063506 (2017), [arXiv:1611.00757 \[astro-ph.CO\]](#) .
- [57] A. H. Guth, *Phys. Rev. D* **23**, 347 (1981).
- [58] A. D. Linde, *Phys. Lett. B* **108**, 389 (1982).
- [59] A. Albrecht and P. J. Steinhardt, *Phys. Rev. Lett.* **48**, 1220 (1982).
- [60] A. A. Starobinsky, *Phys. Lett. B* **91**, 99 (1980).
- [61] A. R. Liddle, P. Parsons, and J. D. Barrow, *Phys. Rev. D* **50**, 7222 (1994).
- [62] E. W. Kolb and M. S. Turner, *The Early Universe*, Vol. 69 (1990).
- [63] L. Kofman, A. D. Linde, and A. A. Starobinsky, *Phys. Rev. D* **56**, 3258 (1997), [arXiv:hep-ph/9704452](#) .
- [64] B. A. Bassett, S. Tsujikawa, and D. Wands, *Rev. Mod. Phys.* **78**, 537 (2006).
- [65] R. Allahverdi, R. Brandenberger, F.-Y. Cyr-Racine, and A. Mazumdar, *Ann. Rev. Nucl. Part. Sci.* **60**, 27 (2010), [arXiv:1001.2600 \[hep-th\]](#) .
- [66] M. A. Amin, M. P. Hertzberg, D. I. Kaiser, and J. Karouby, *Int. J. Mod. Phys. D* **24**, 1530003 (2014), [arXiv:1410.3808 \[hep-ph\]](#) .
- [67] M. Drewes, J. U. Kang, and U. R. Mun, *JHEP* **11**, 072 (2017), [arXiv:1708.01197 \[astro-ph.CO\]](#) .
- [68] M. R. Haque and D. Maity, *Phys. Rev. D* **107**, 043531 (2023), [arXiv:2201.02348 \[hep-ph\]](#) .
- [69] J. L. Cook, E. Dimastrogiovanni, D. A. Easson, and L. M. Krauss, *JCAP* **04**, 047 (2015), [arXiv:1502.04673 \[astro-ph.CO\]](#) .
- [70] M. R. Haque and D. Maity, *Phys. Rev. D* **107**, 043531 (2023).
- [71] L. Dai, M. Kamionkowski, and J. Wang, *Phys. Rev. Lett.* **113**, 041302 (2014).
- [72] J. Martin and C. Ringeval, *Phys. Rev. D* **82**, 023511 (2010).
- [73] D. Maity and P. Saha, *Phys. Rev. D* **98**, 103525 (2018).
- [74] D. Maity, S. Pal, and T. Paul, *JCAP* **05**, 045 (2021), [arXiv:2103.02411 \[hep-th\]](#) .
- [75] A. Chakraborty, S. Maiti, and D. Maity, *Phys. Rev. D* **111**, 083505 (2025), [arXiv:2408.07767 \[astro-ph.CO\]](#) .
- [76] T. Kahniashvili, A. Brandenburg, R. Durrer, A. G. Tevzadze, and W. Yin, *JCAP* **12**, 002 (2017), [arXiv:1610.03139 \[astro-ph.CO\]](#) .
- [77] A. Benevides, A. Dabholkar, and T. Kobayashi, *JHEP* **11**, 039 (2018), [arXiv:1808.08237 \[hep-th\]](#) .
- [78] T. Kobayashi and M. S. Sloth, *Phys. Rev. D* **100**, 023524 (2019), [arXiv:1903.02561 \[astro-ph.CO\]](#) .
- [79] D. Paoletti, J. Chluba, F. Finelli, and J. Rubiño-Martín, *Monthly Notices of the Royal Astronomical Society* **517**, 3916 (2022).
- [80] C. Caprini, R. Durrer, and T. Kahniashvili, *Phys. Rev. D* **69**, 063006 (2004).
- [81] J. L. Cook and L. Sorbo, *Phys. Rev. D* **85**, 023534 (2012).
- [82] A. Lewis, *Phys. Rev. D* **70**, 043011 (2004).
- [83] T. J. Clarke, E. J. Copeland, and A. Moss, *JCAP* **10**, 002 (2020), [arXiv:2004.11396 \[astro-ph.CO\]](#) .
- [84] I. Sendra and T. L. Smith, *Phys. Rev. D* **85**, 123002 (2012).
- [85] C. Caprini and D. G. Figueroa, *Class. Quant. Grav.* **35**, 163001 (2018), [arXiv:1801.04268 \[astro-ph.CO\]](#) .
- [86] T. J. Clarke, E. J. Copeland, and A. Moss, *Journal of Cosmology and Astroparticle Physics* **2020**, 002 (2020).
- [87] N. Aghanim *et al.* (Planck), *Astron. Astrophys.* **641**, A6 (2020), [Erratum: *Astron. Astrophys.* 652, C4 (2021)], [arXiv:1807.06209 \[astro-ph.CO\]](#) .
- [88] A. et al, *arXiv e-prints*, [arXiv:2306.16224 \(2023\)](#), [arXiv:2306.16224 \[astro-ph.HE\]](#) .
- [89] A. Mitridate, D. Wright, R. von Eckardstein, T. Schröder, J. Nay, K. Olum, K. Schmitz, and T. Trickle, *arXiv e-prints*, [arXiv:2306.16377 \(2023\)](#), [arXiv:2306.16377 \[hep-ph\]](#) .